

## SUPPORTING INFORMATION

### **MgO-Supported Iridium Metal Pair-Site Catalysts are More Active and Resistant to CO Poisoning than Analogous Single-Site Catalysts for Ethylene Hydrogenation and H-D Exchange**

Erjia Guan,<sup>a</sup> Louise Debeve,<sup>b</sup> Monica Vasiliu,<sup>c</sup> Shengjie Zhang,<sup>c</sup> David A. Dixon,<sup>c</sup> and Bruce C. Gates<sup>b,\*</sup>

<sup>a</sup>Department of Materials Science and Engineering, University of California, Davis, California 95616, United States

<sup>b</sup>Department of Chemical Engineering, University of California, Davis, California 95616, United States

<sup>c</sup>Department of Chemistry, University of Alabama, Tuscaloosa, Alabama 35487, United States

Email: bcgates@ucdavis.edu

## EXPERIMENTAL AND COMPUTATIONAL METHODS

### Synthesis of iridium pair-site catalyst supported on MgO

The MgO support (Matheson, Coleman, & Bell, 3–5 g per calcination batch) was calcined in O<sub>2</sub> at 973 K for 2 h and followed by evacuation at 973 K for 14 h. The precursor Ir<sub>2</sub>(μ-OMe)<sub>2</sub>(COD)<sub>2</sub> (99%, Strem) was mixed with the calcined MgO (e.g., to give 0.8 wt% iridium on support, 13.8 mg of precursor was mixed with 1.0 g of MgO) in dried, deoxygenated *n*-pentane solvent (Fisher, 99%, 100–150 mL) and stirred for 24 h at 298 K and 1 bar. The solvent was removed by evacuation for 24 h. All procedures were done with air- and moisture-exclusion techniques. The procedure left all the iridium in the catalyst.

### IR spectroscopy and mass spectrometry

IR spectra were recorded with a Bruker IFS 66v/S spectrometer with a resolution of 2 cm<sup>-1</sup> and an average of 64 scans. Each sample (~30 mg, handled with exclusion of air and moisture) was pressed into a thin wafer and loaded into a flow cell (In-situ Research Institute, KBr windows). The cell was sealed in an argon-filled glovebox and connected to a flow system that allowed recording of spectra while gases passed through and around the wafer. The mass spectrometer was connected to the flow system that included the IR cell. Mass spectra of effluent gases from the reactor/IR cell were measured with an on-line Balzers OmniStar™ mass spectrometer running in multi-ion monitoring mode. The changes in the signal intensities of the main fragments of H<sub>2</sub> ( $m/z$  = 2), HD ( $m/z$  = 3), and D<sub>2</sub> ( $m/z$  = 4) were recorded.

## X-ray Absorption Spectroscopy (EXAFS and XANES)

Transmission XANES and EXAFS spectra were measured at SSRL Beamline 4-1 and with the high-energy-resolution X-ray fluorescence detector used for high energy-resolution XANES at SSRL beamline 6-2. Each sample (300 mg) was mixed with dry boron nitride (200 mg) and packed into a flow-through cell in an argon-filled glovebox. The measurements were made at 298 K. HERFD scans were recorded every 2 min.

Analysis of the XANES and EXAFS data was carried out with the software ATHENA of the IFEFFIT package,<sup>1</sup> and the EXAFS data were further analyzed with the software XDAP developed by Vaarkamp *et al.*<sup>2</sup> Three spectra were averaged to give each spectrum that was subjected to analysis. The error in the data was calculated as the root mean square of the value obtained from the subtraction of smoothed  $\chi$  ( $\chi$  is the EXAFS function) data from the background-subtracted experimental  $\chi$  values. Goodness of fit values was calculated with the software XDAP, as follows:

$$\text{Goodness of fit} = \frac{\nu}{\text{NPTS}(\nu - N_{\text{free}})} \sum_{i=1}^{\text{NPTS}} \left( \frac{\chi_{\text{exp},i} - \chi_{\text{model},i}}{\sigma_{\text{exp},i}} \right)^2 \quad (\text{S1})$$

In equation S1,  $\chi_{\text{model}}$  and  $\chi_{\text{exp}}$  are the model and experimental EXAFS values;  $\sigma_{\text{exp}}$  is the error in the experimental results;  $\nu$  is the number of independent data points in the fit range; and NPTS is the actual number of data points in the fit range;  $N_{\text{free}}$  is the number of free parameters.

A "difference-file" technique was applied to the candidate models, whereby the calculated EXAFS contribution from each individual Ir-backscatterer contribution was compared with the data in  $R$  (distance) space (calculated by subtracting all the other calculated Ir-backscatterer contributions from the experimental overall contributions).

The best-fit model is the one providing optimum agreement between the model and the calculated EXAFS data in  $k$  space and in  $R$  space, also for the individual shells.

### **Scanning Transmission Electron Microscopy (STEM)**

STEM imaging was performed on a JEOL JEM-2100F electron microscope equipped with a CEOS hexapole aberration corrector. The microscope was equipped with a field emission gun and operated at 200 kV. The high-angle annular dark field images were obtained with a probe convergence angle of 34.2 mrad. The samples were prepared for imaging in an argon-filled glovebox with concentrations of  $\text{H}_2\text{O} < 0.5$  ppm and  $\text{O}_2 < 5$  ppm. A lacey carbon grid (300 mesh, Ted Pella) was dipped into the powder, so that a small amount of dispersed sample adhered to the grid, minimizing overlap of MgO particles to facilitate interpretation and minimize charging during imaging. The grid was loaded onto a vacuum transfer holder (Fischione model 2020) before introduction into the microscope.

### **Density Functional Theory (DFT) Calculations**

The geometries were optimized and frequencies were calculated with DFT<sup>3</sup> using the  $\omega$ B97X-D<sup>4</sup> functional and the DZVP2(C,O,H),<sup>5</sup> cc-pVDZ(Mg),<sup>6</sup> and cc-pVDZ-PP(Ir)<sup>7</sup> basis sets. All calculations were done with Gaussian-16.<sup>8</sup>

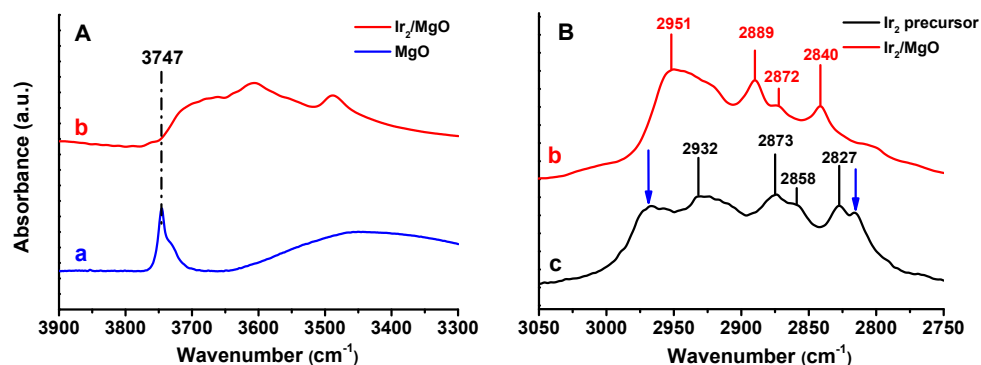
### **Catalytic Reaction Rate Measurements**

Ethylene hydrogenation was performed in a conventional quartz laboratory once-through tubular plug-flow reactor. The catalyst powder (12–100 mg) was mixed with 5.0 g of inert  $\alpha$ - $\text{Al}_2\text{O}_3$  powder and sealed in the reactor in an argon-filled glovebox. The catalytic reaction took place at various temperatures and at atmospheric pressure

with a total feed flow rate of 100 mL(NTP)/min. Various  $\text{C}_2\text{H}_4/\text{H}_2$  molar ratios were used (1, 0.25 or 4), and the partial pressures of  $\text{C}_2\text{H}_4$  and  $\text{H}_2$  were (1) both 200 mbar; (2) 100 mbar and 400 mbar and (3) 400 mbar and 100 mbar balanced with flowing helium to reach 1 bar in total.

The effluent stream was analyzed with a gas chromatograph (Agilent HP-6890) equipped with a capillary column (PLOT Alumina "M", 50 m  $\times$  0.53 mm) and a flame-ionization detector. Each scan took 10 min. The ethylene conversions were  $< 5\%$ , and the reactor was approximated as differential.

## Initial Structures of Iridium Pair-sites on MgO



**Supporting Figure S1.** IR spectra of A,  $\nu_{\text{O-H}}$  and B,  $\nu_{\text{C-H}}$  regions of (a) MgO; (b) sample after chemisorption of  $\text{Ir}_2(\mu\text{-OMe})_2(\text{COD})_2$  on MgO; (c)  $\text{Ir}_2(\mu\text{-OMe})_2(\text{COD})_2$  precursor mixed with KBr.

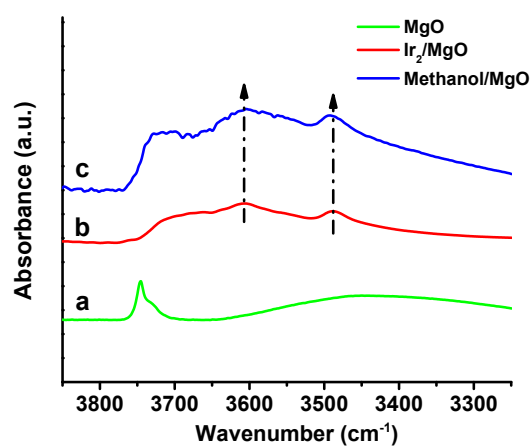
**Note:** The band assigned to OH groups on MgO (at  $3747\text{ cm}^{-1}$ ) declined in intensity as  $\text{Ir}_2(\mu\text{-OMe})_2(\text{COD})_2$  reacted with them (Figure S1A). The bands assigned to the C–H vibrations in the cyclooctadiene<sup>9</sup> in the adsorbed species (Figure S1B, c), at  $2932$ ,  $2873$ ,  $2858$ , and  $2827\text{ cm}^{-1}$ , were blue shifted by about  $17\text{ cm}^{-1}$  upon adsorption of  $\text{Ir}_2(\mu\text{-OMe})_2(\text{COD})_2$  (Figure S1B, b), consistent with the role of the support as a ligand influencing the electron density on iridium and it is further confirmed by DFT calculations in Table S1. The  $2967\text{ cm}^{-1}$  band characteristic of C–H vibrations in COD ligands with  $\text{C}_{2v}$  symmetry bonded to metal centers such as Rh or Pd<sup>10</sup> in crystalline state was not detectable in the spectrum of the supported species, consistent with a break in symmetry resulting from the adsorption. A band characteristic of C–H vibrations in bridging methoxy ligands on metals such as Ni or Ti (at  $2800\text{--}2816\text{ cm}^{-1}$ )<sup>11</sup> is evident in the spectrum of  $\text{Ir}_2(\mu\text{-OMe})_2(\text{COD})_2$  at  $2815\text{ cm}^{-1}$ , and it disappeared as a result of the chemisorption, indicating that methoxy ligands were all removed from the iridium.

**Supporting Table S1.** C-H Stretch Frequencies (cm<sup>-1</sup>) and IR intensities (km/mol) for COD groups at  $\omega$ B97xD//DZVP2(C,O)/cc-pVDZ(Mg)/cc-pVDZ-PP(Ir).

Ir <sub>2</sub> (COD) <sub>2</sub> (CH <sub>3</sub> O) <sub>2</sub>		Ir <sub>2</sub> (COD) <sub>2</sub> (MgO) <sub>25</sub>		Ir <sub>2</sub> (COD) <sub>2</sub> (MgO) <sub>25</sub> (Ir top O)		Ir <sub>2</sub> O <sub>2</sub> (COD) <sub>2</sub> (MgO) <sub>25</sub> <sup>-2</sup>		Ir <sub>2</sub> (OH) <sub>2</sub> (COD) <sub>2</sub> (MgO) <sub>25</sub>	
Freq. <sup>a</sup>	Intens.	Freq.	Intens.	Freq.	Intens.	Freq.	Intens.	Freq.	Intens.
3043.5	95.4	3047.3	93.5	3050.3	49.0	3011.9	94.7	3061.7	46.4
3046.4	72.2	3059.2	58.9	3058.1	74.7	3013.3	95.5	3063.3	70.3
3066.1	55.4	3060.5	26.4	3059.6	44.3	3017.6	97.0	3065.2	36.4
3066.2	96.2	3060.9	62.3	3065.1	67.4	3018.8	139.7	3069.3	57.1
3067.6	45.2	3078.2	148.2	3072.4	65.8	3036.6	285.1	3078.7	100.4
3068.0	43.3	3079.5	78.0	3087.8	108.3	3037.3	50.0	3097.0	31.8
3101.9	25.1	3085.8	81.5	3091.9	39.1	3066.6	54.1	3100.2	26.0
3101.9	31.4	3094.1	40.7	3093.9	2.4	3067.7	59.2	3101.1	90.0
3107.4	173.2	3095.9	69.9	3097.0	38.4	3073.1	116.5	3104.0	51.7
3107.9	49.4	3102.2	31.4	3102.3	139.3	3074.0	184.2	3107.0	22.3
<b>3121.6</b>	42.7	3107.6	21.2	3107.3	2.9	3084.6	1.3	3109.7	24.5
3122.2	16.0	3109.9	9.7	3110.3	3.3	3087.8	15.3	3111.7	13.4
3122.7	0.6	3115.7	21.0	3113.4	21.5	3104.9	19.9	3115.6	23.9
3123.8	5.9	3117.0	5.9	3120.4	16.3	3107.5	30.1	3116.1	32.3
3123.9	17.0	3121.8	19.0	3126.1	38.3	3108.1	38.6	3122.3	15.0
<b>3124.7</b>	38.7	3132.4	56.0	3127.1	55.9	3113.0	51.2	3122.8	32.5
3143.3	9.5	3132.6	116.7	3130.2	41.7	3113.3	43.2	3129.3	27.3
3143.5	13.4	3136.3	11.0	3139.4	43.4	3115.5	39.1	3136.0	35.4
<b>3144.6</b>	24.6	3141.8	22.3	3141.6	20.8	3122.0	12.2	3138.9	29.0
<b>3148.0</b>	29.5	3158.0	28.3	3150.2	31.4	3126.0	9.8	3140.4	13.9
3149.2	14.3	3174.1	6.0	3171.7	7.8	3147.1	60.7	3144.7	47.1
3149.5	0.7	3183.1	24.4	3173.6	26.1	3148.3	24.9	3155.5	50.8
3153.8	9.5	3191.6	12.7	3202.5	21.1	3157.6	37.4	3156.8	36.6
3153.9	26.0	3228.3	8.9	3309.5	0.6	3160.1	39.2	3198.3	5.0
3155.8	26.9								
3156.2	86.8								
3167.6	1.4								
3168.2	158.8								
3173.9	23.8								
3174.1	9.4								

<sup>a</sup> In red values for the  $\nu_{\text{CH}}$  vibration in O-CH<sub>3</sub> group.

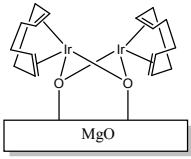
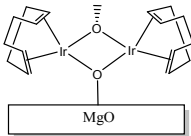
The data give the expected differences between the calculated harmonic values and the experimental anharmonic ones.



**Supporting Figure S2.** IR spectra of  $\nu_{\text{O-H}}$  region of (a) MgO, (b) sample after chemisorption of  $\text{Ir}_2(\mu\text{-OMe})_2(\text{COD})_2$  on MgO, and (c) MgO in brought in contact with methanol vapor with helium carrier gas sparged through a methanol solution at 298 K and 1 bar.



**Supporting Table S2.** EXAFS structure parameters<sup>a</sup> representing MgO-supported species formed by adsorption of Ir<sub>2</sub>(μ-OMe)<sub>2</sub>(COD)<sub>2</sub>.

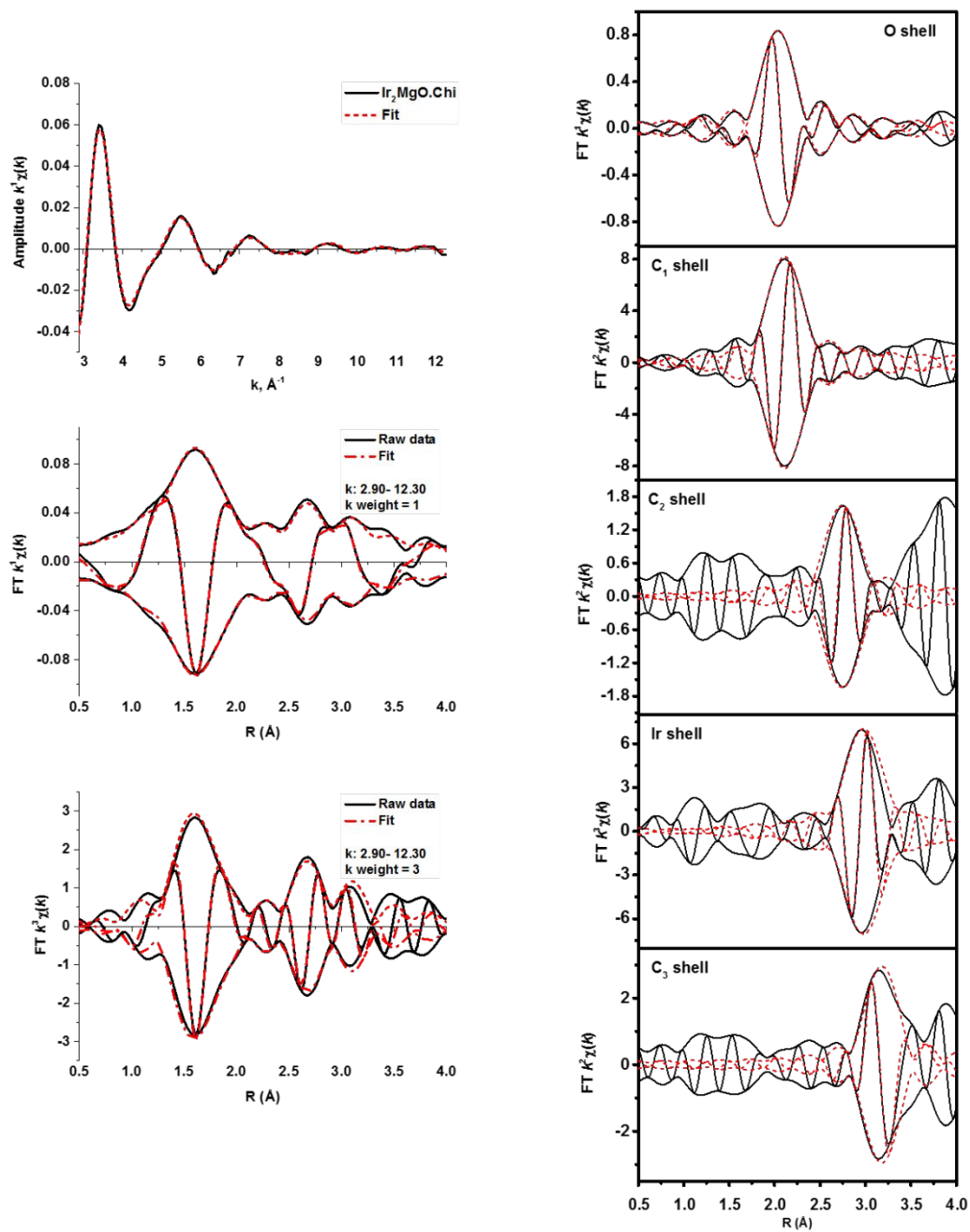
Proposed Structure	Shell	<i>N</i>	<i>R</i> (Å)	$10^3 \times \sigma^2$ (Å <sup>2</sup> )	$\Delta E_0$ (eV)	Goodness of Fit
Model 1	Ir–O <sub>s</sub>	1.9	1.99	0.6	-9.0	
	Ir–Ir	0.95	2.99	3.2	3.3	
	Ir–C <sub>COD1</sub>	3.8	2.13	1.7	8.6	0.51
	Ir–C <sub>COD2</sub>	1.2	2.76	1.3	3.1	
	Ir–C <sub>COD2</sub>	3.1	3.11	3.3	-9.9	
Model 2	Ir–O <sub>OMe</sub>	1.0	1.97	1.4	-9.1	
	Ir–O <sub>s</sub>	1.0	2.03	0.9	-13.3	
	Ir–Ir	0.91	3.03	2.5	-8.6	0.90
	Ir–C <sub>COD1</sub>	4.0	2.14	2.3	6.9	
	Ir–C <sub>COD2</sub>	3.8	3.16	5.4	-8.9	

<sup>a</sup>Notation: *N*, coordination number; *R*, distance between absorber and backscatterer atoms;  $\sigma^2$ , disorder term (Debye-Waller factor);  $\Delta E_0$ , inner potential correction. Estimated error bounds: *N*,  $\pm 20\%$ ; *R*,  $\pm 0.02$  Å;  $\sigma^2$ ,  $\pm 20\%$ ;  $\Delta E_0$ ,  $\pm 20\%$ ; *k* range: 2.9-12.3 Å<sup>-1</sup>; error: 0.0018. O<sub>s</sub>: O in MgO; O<sub>OMe</sub>: O in bridging methoxy ligand; C<sub>COD1</sub>: C in cyclooctadiene ligands at bonding distances to Ir; C<sub>COD2</sub>: C in cyclooctadiene ligands at non-bonding distances to Ir.

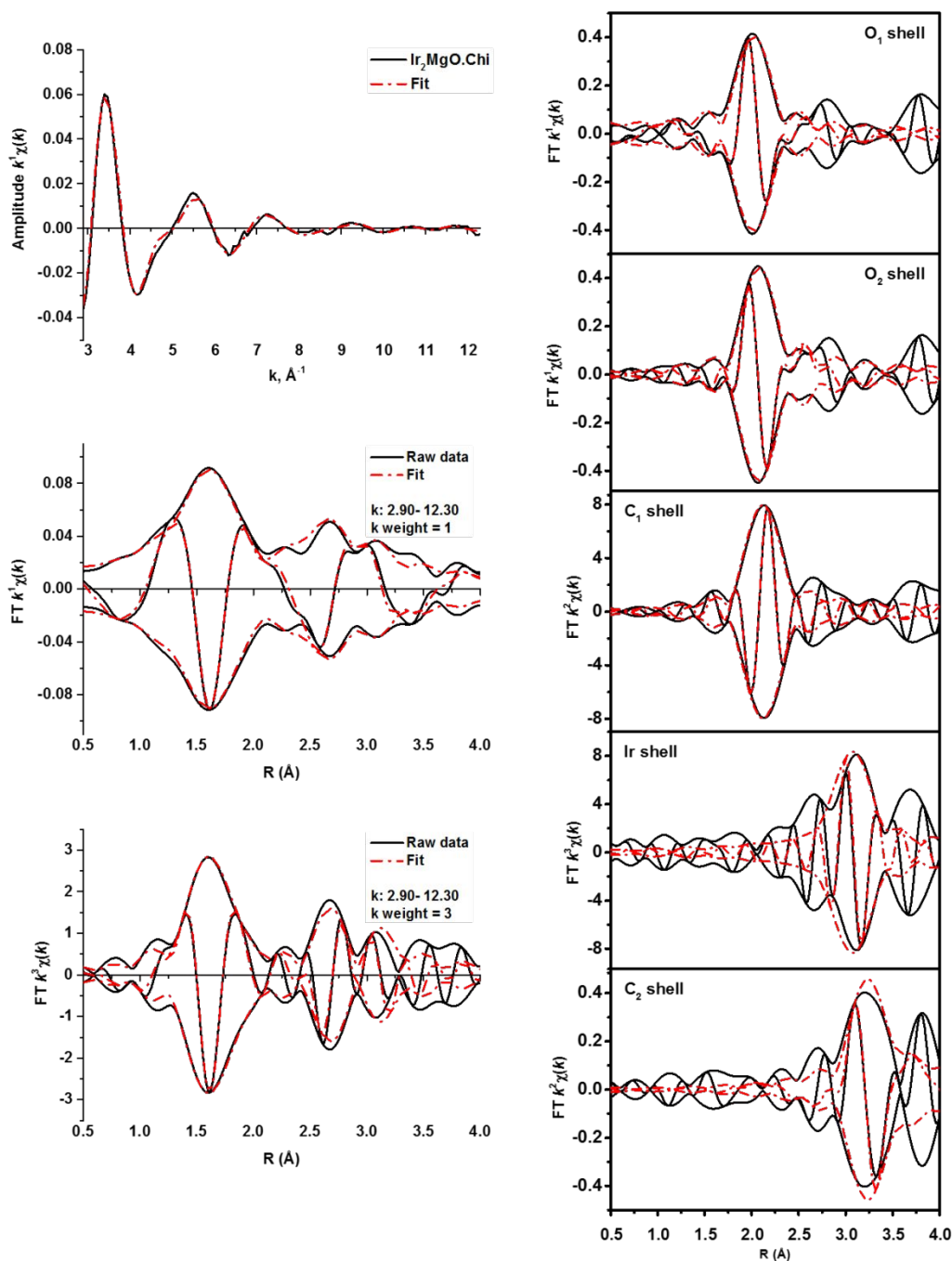
Note: Model 1 and Model 2 both indicate that the coordination number of the Ir–Ir contribution is approximately 1 and at a distance close to 3.0 Å; and the coordination number of Ir–O contribution is 2 at a distance close to 2.0 Å (in Model 2 we separate two Ir–O shells belonging to support oxygen atoms and oxygen atoms in methoxy ligands); both coordination numbers of the Ir–C<sub>COD1</sub> shell, which represent  $\pi$ -bonded carbon, are approximately 4 in both models, at a distance close to 2.1 Å, confirming that COD ligands remain on Ir after the chemisorption. We separated the Ir–C<sub>COD2</sub> shells which represent different carbon atoms in COD ligands appearing at a non-bonding distance from Ir in Model 1. Model 1 gives a better fit in *k* space, *R* space, and in each individual shell, shown by better goodness of fit values. We chose Model 1 also in part

with the awareness that it gives a better illustration of the complexity of COD ligand conformation than the other model.

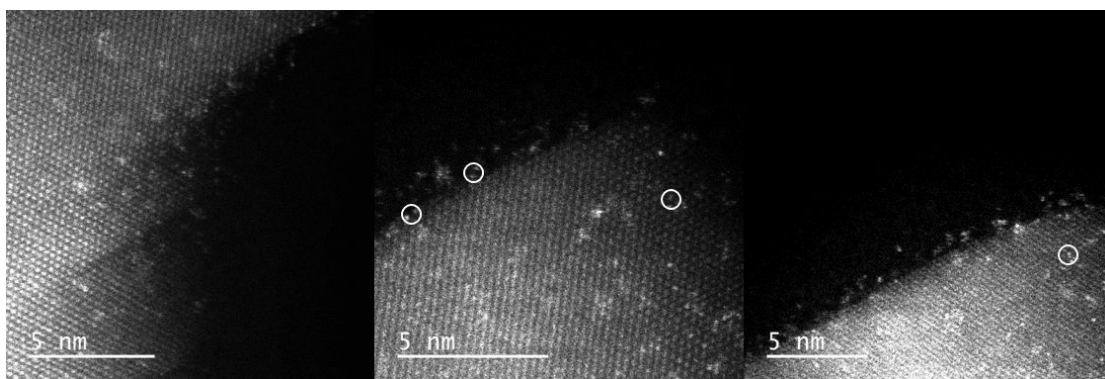
# (A) Model 1



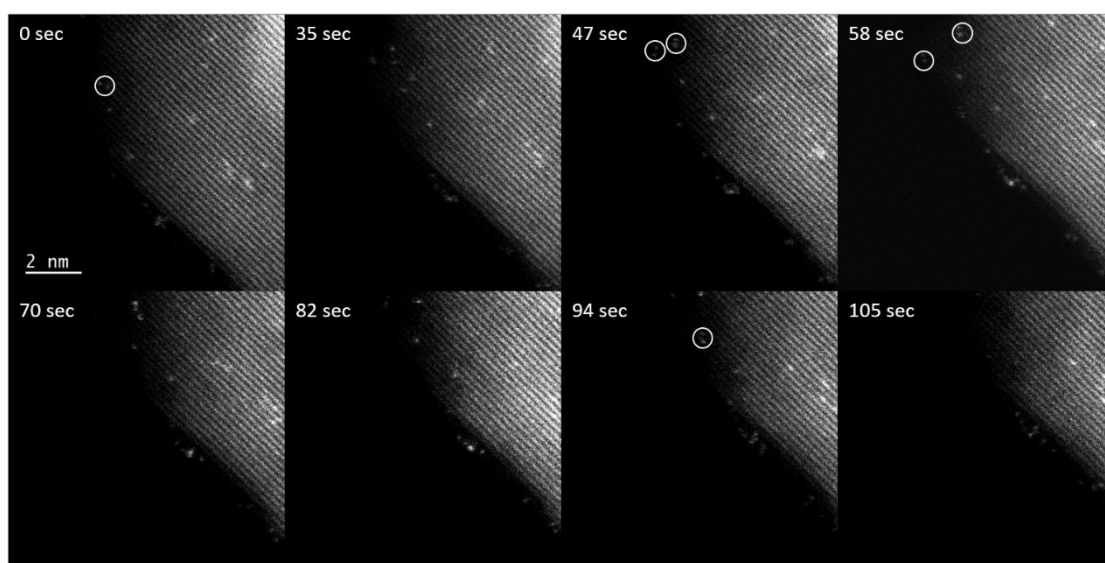
(B) Model 2



**Supporting Figure S3.** EXAFS (A) model 1 and (B) model 2 characterizing Ir<sub>2</sub>/MgO:  $k^1$ -weighted EXAFS function,  $k^1(\chi)$  (solid line) and sum of the calculated contributions (dashed line);  $k^1$ -weighted and  $k^3$ -weighted and single shell imaginary part and magnitude of the Fourier transform of the data (solid line) and sum of the calculated contributions (dashed line) of the samples.



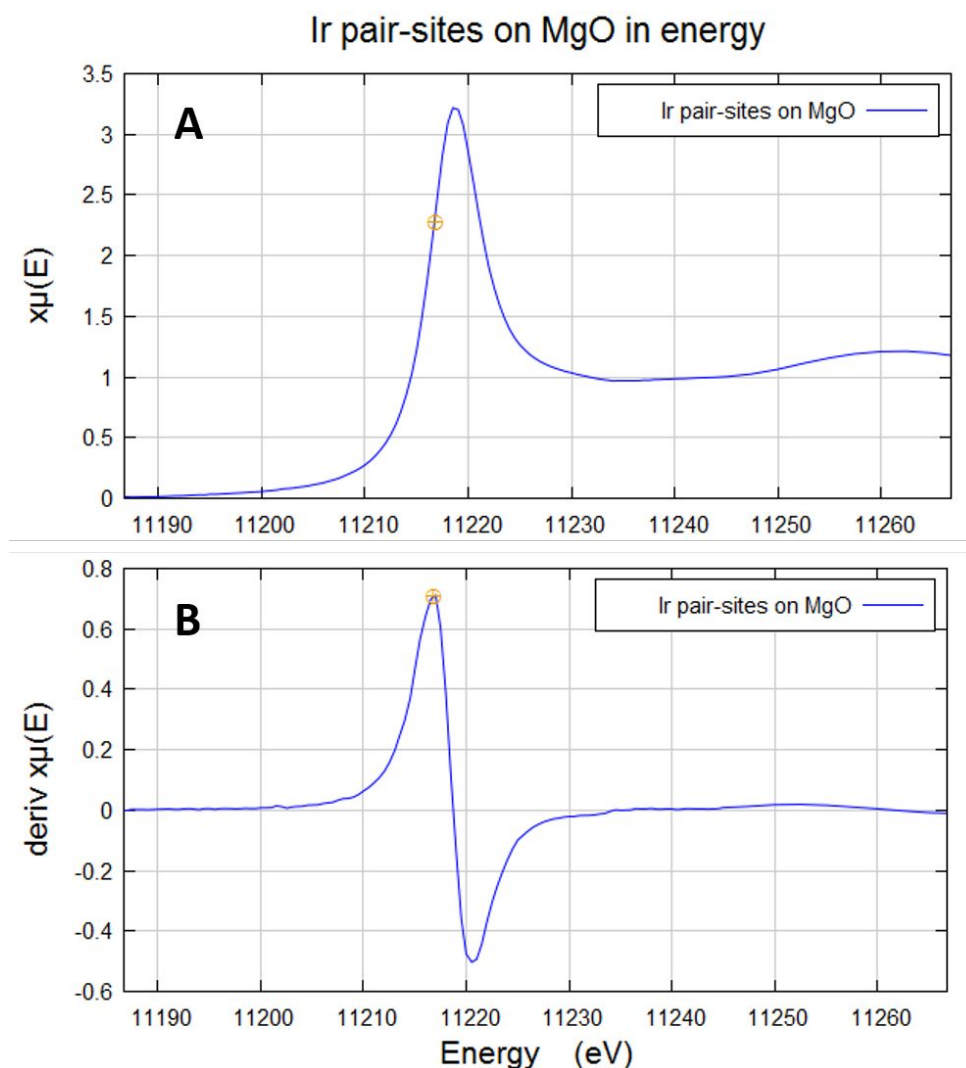
**Supporting Figure S4.** Additional HAADF-STEM images showing that the iridium species were predominantly present as in single and pair sites (circled), the former inferred to have formed under the influence of the electron beam (see main text and following figure). The distance between Ir atoms was measured on the intensity profiles, by measuring the distance between the two points showing the highest intensity. The distances between Ir atoms were measured in images for which the electron beam was parallel to the zone axis of the MgO surface—meaning that the distances measured were unaffected by tilting of the MgO crystals.



**Supporting Figure S5.** Series of consecutive HAADF-STEM images of one area of the sample. The sample was exposed to the electron beam for a total of 105 s and a total dose of  $\sim 10^6 \text{ e}^- \text{ \AA}^{-2}$ . Iridium dimers are circled. The beam broke up the iridium pair-sites and caused movement of Ir atoms on the MgO surface, forming and breaking up dimer-like species. The Ir atoms did not form bigger clusters in the time of the experiment, although the dose was similar to doses known to cause sintering of iridium species.<sup>12</sup>

Note: As illustrated in Figure S5, prolonged exposure to the electron beam initially caused dimer break-up, and then movement of the Ir atoms. There was no evidence of cluster formation under the influence of the electron beam. Instead, the Ir atoms

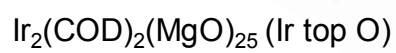
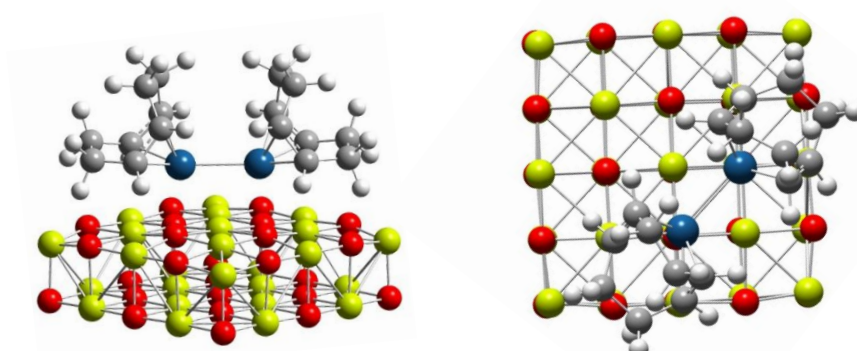
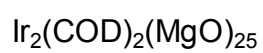
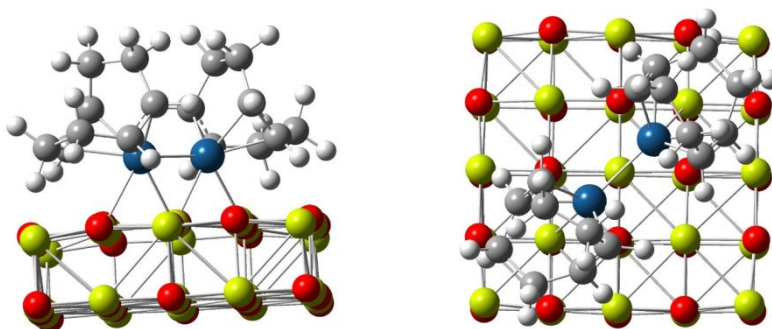
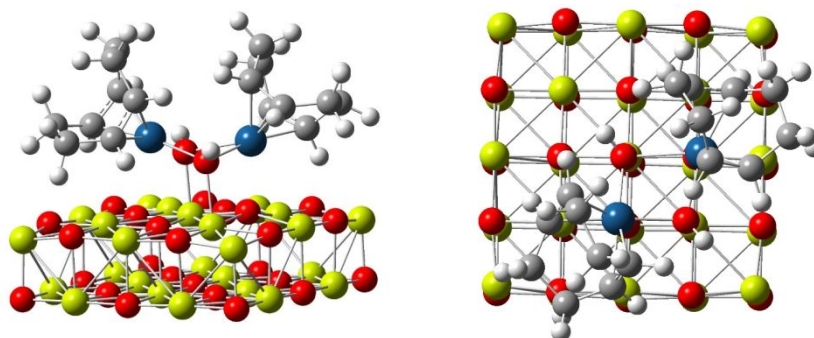
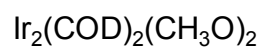
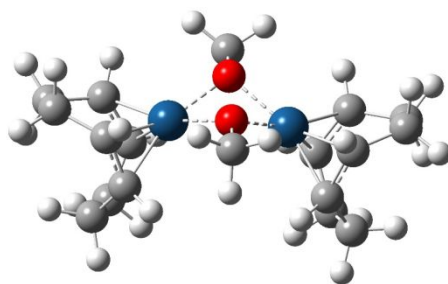
appeared to bounce off each other, as illustrated in Figure S5. In the first frame, the iridium is present as site-isolated species. It is shown to be in different locations in the following frames. In the frames recorded at 47 and 58 s, there are pair-sites present (circled). Those pair-sites broke up and were not evident in the subsequent frames.



**Supporting Figure S6.** (A) XANES spectra and (B) the first derivative of the XANES spectra characterizing iridium pair-sites on MgO. The edge position of Ir in the pair-sites is 11216.7 eV.

### **Additional DFT models of the iridium pair-sites:**

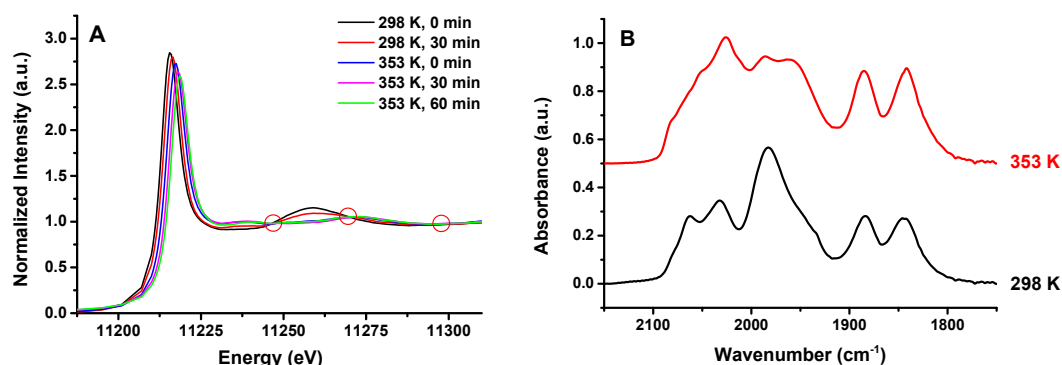
In addition to the models for  $\text{Ir}_2(\text{COD})_2\text{R}_n$  bonded to MgO described in the text, additional models were studied. In one model, the  $\text{CH}_3\text{O}$  groups were removed from  $\text{Ir}_2(\text{COD})_2(\text{CH}_3\text{O})_2$ , and each Ir atom was bonded to a MgO cluster surface. Two structures were then optimized, one with each Ir over a surface O atom ( $\text{Ir}_2(\text{COD})_2(\text{MgO})_{25}$  (Ir top O)) and one with each Ir atom between two surface O atoms ( $\text{Ir}_2(\text{COD})_2(\text{MgO})_{25}$ ); these structures are essentially isoenergetic. The Ir–O and Ir–Ir bond distance of the first structure are 2.26 and 2.77 Å, respectively. The second structure has a short Ir–O distance of 2.30 Å and a longer one of 3.06 Å with an Ir–Ir distance of 2.78 Å. Neither of these is in particularly good agreement with the EXAFS data. As a benchmark, the structure of  $\text{Ir}_2(\mu\text{-OMe})_2(\text{COD})_2$  was calculated with an Ir–O bond distance of 2.08 Å and an Ir–Ir distance of 3.00 Å, consistent with the crystal structure values.<sup>13</sup>



**Supporting Figure S7.** Additional DFT candidate models described in the manuscript and Supporting Information, top and side views.

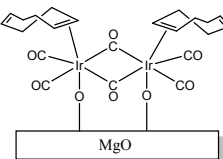
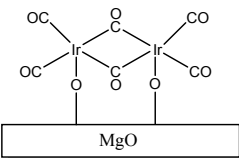
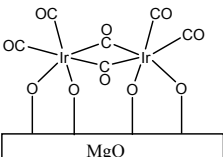


## Reactivity of Iridium Pair-sites towards CO



**Supporting Figure S8.** (A) XANES spectra characterizing iridium pair-sites on MgO exposed to continuously flowing CO (10% CO in He, flow rate = 50 mL/min) at 298 K for 30 min until no further changes in the XANES region ensued, followed by an increase in the temperature to 353 K and holding at this temperature for 1 h, after which there was no further change in the spectrum. (B) IR spectra in the  $\nu_{\text{CO}}$  region characterizing iridium pair-sites on MgO exposed to flowing CO for 1 h at 298 K or 353 K, respectively, and followed by exposure to flowing helium purge out residual gaseous CO. The isosbestic points in the XANES spectra (red circles) demonstrate stoichiometrically simple transformations.

**Supporting Table S3.** EXAFS structure parameters<sup>a</sup> representing MgO-supported species formed by adsorption of Ir<sub>2</sub>(μ-OMe)<sub>2</sub>(COD)<sub>2</sub> treated by flowing CO (50 mL(NTP)/min) at 298 K and 353 K for 1 h.

Sample and Proposed structure	Shell	<i>N</i>	<i>R</i> (Å)	10 <sup>3</sup> × σ <sup>2</sup> (Å <sup>2</sup> )	Δ <i>E</i> <sub>0</sub> (eV)	Goodness of Fit
Ir <sub>2</sub> /MgO after exposure to flowing CO (flow rates: CO, 5; He, 45 mL/min) at 298 K for 1 h  	Ir–O <sub>s</sub>	1.1	2.02	1.0	-8.0	
	Ir–C <sub>COD+CO</sub>	4.0	2.19	4.7	-5.1	
	Ir–C <sub>br</sub>	2.1	2.39	0.1	3.4	6.44
	Ir–Ir	1.2	2.75	2.1	7.2	
	Ir–O <sub>CO</sub>	4.1	2.88	2.9	0.7	
Ir <sub>2</sub> /MgO after exposure to flowing CO (flow rates: CO, 5; He, 45 mL/min) at 353 K for 1 h.   Model 1	Ir–Ir	0.96	2.80	2.4	7.9	
	Ir–O <sub>s</sub>	0.90	2.25	1.9	1.1	
	Ir–C <sub>ter</sub>	1.8	2.04	5.5	-11	4.37
	Ir–O <sub>CO</sub>	4.3	2.96	2.4	-3.6	
	Ir–C <sub>br</sub>	1.9	2.11	1.8	1.0	
 Model 2	Ir–C <sub>ter</sub>	1.9	1.98	8.1	-5.8	
	Ir–O <sub>s</sub>	2.0	2.07	3.9	2.7	
	Ir–C <sub>br</sub>	1.9	2.28	5.0	8.7	5.22
	Ir–Ir	0.91	2.80	3.0	7.4	
	Ir–O <sub>CO</sub>	4.0	2.93	5.2	-2.6	

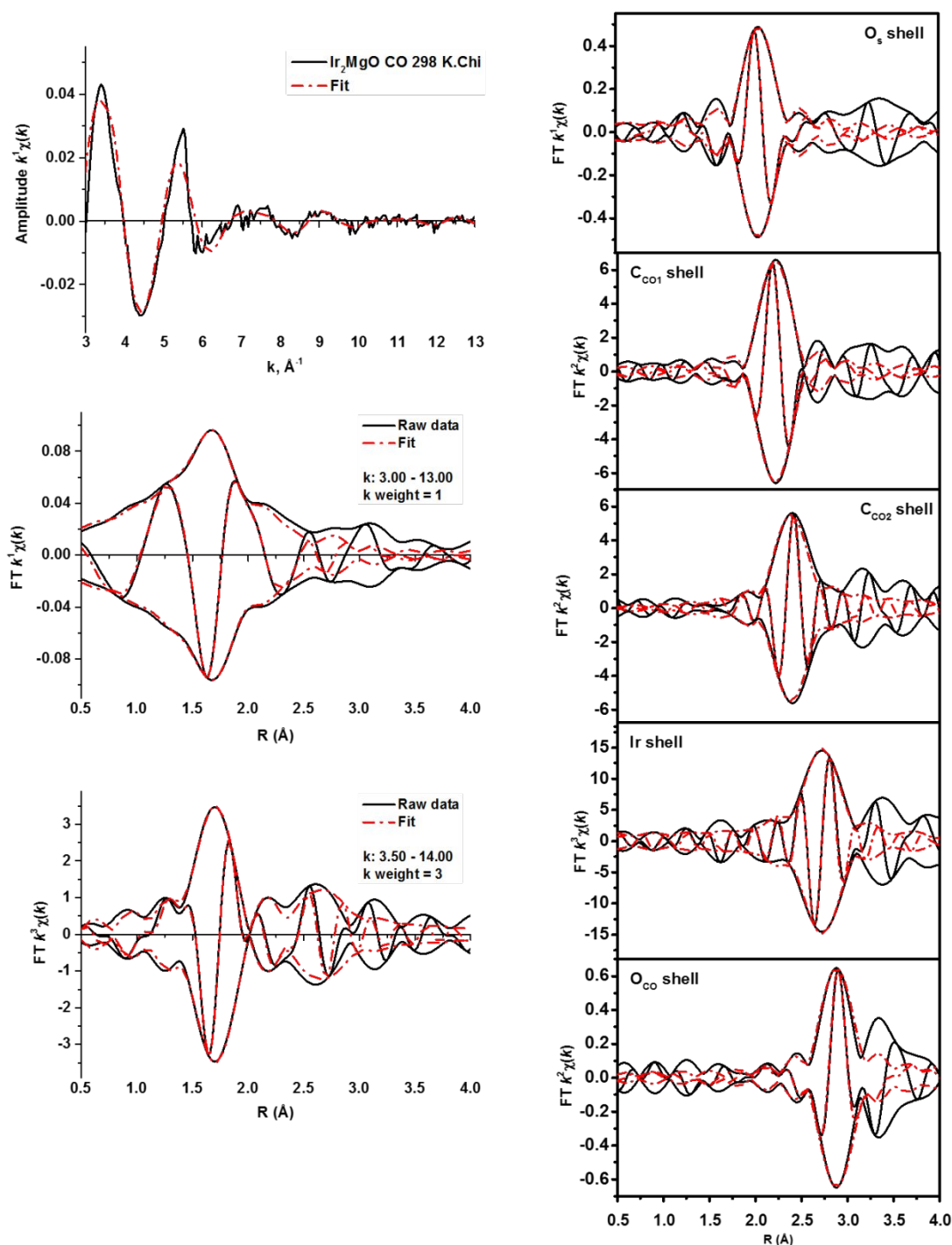
<sup>a</sup>Notation: *N*, coordination number; *R*, distance between absorber and backscatterer atoms; σ<sup>2</sup>, disorder term (Debye-Waller factor); Δ*E*<sub>0</sub>, inner potential correction. Estimated error bounds: *N*, ± 20%; *R*, ± 0.02 Å; σ<sup>2</sup>, ± 20%; Δ*E*<sub>0</sub>, ± 20%. *k* range: 3.0-13.0 Å<sup>-1</sup>; error: 0.0012. O<sub>s</sub>: O in MgO; O<sub>CO</sub>: O in CO ligands; C<sub>COD+CO</sub>: C in cyclooctadiene and terminal CO ligands; C<sub>br</sub>: C in bridging CO ligands.

Note: The Ir–Ir coordination number remained essentially unchanged and equal within error to 1 during the CO treatment at 298 K or 353 K. The data showed the Ir–O coordination number approximately 1 and showed that some oxygen-containing ligands in the initial sample were replaced by CO during the treatment. The coordination

number of the Ir–C shell representing terminal CO ligands increased from approximately 2 to 3 when the temperature increased from 298 to 353 K, consistent with full replacement of the cyclooctadiene ligands by CO at the higher temperature. The coordination number of the Ir–bridging carbon shell remained essentially unchanged and nearly equal to 2 at both temperatures. The sample exposed to flowing CO at only 298 K was only partly converted, and the data were not sufficient to distinguish cyclooctadiene and terminal and bridging CO.

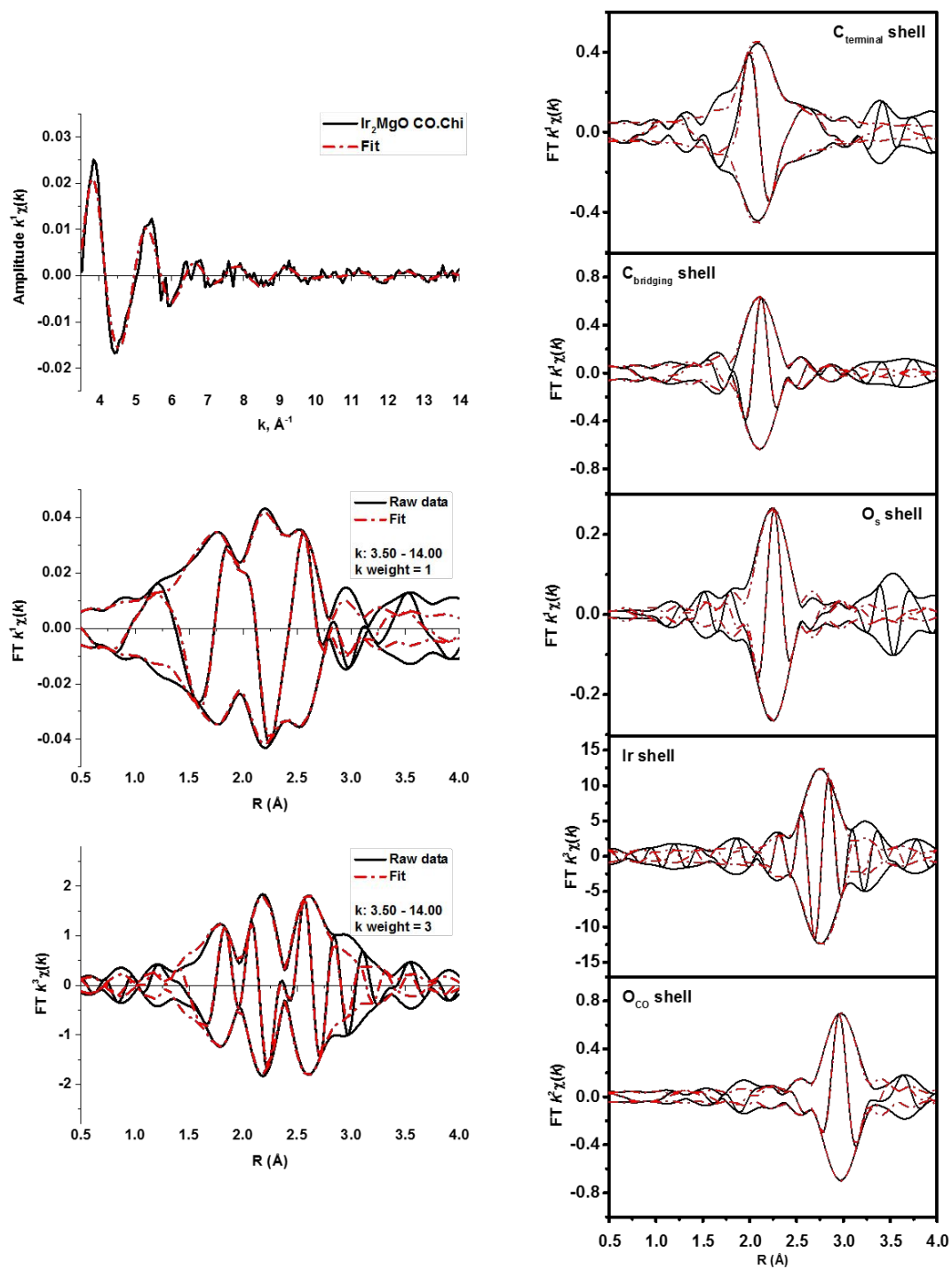
Two models were tested to represent the EXAFS data characterizing the sample exposed to CO at 353 K, with all the organic ligands replaced by CO. Model 1 corresponds to the bonding of each Ir atom to one oxygen atom of MgO, three terminal CO ligands, and two bridging CO ligands; Model 2 corresponds to the bonding of each Ir atom to two support oxygen atoms, two terminal CO ligands, and two bridging CO ligands. Model 1 gives a substantially better fit than model 2 in k space, R space and each individual shell (Figure S11).

## CO treated Ir pair-sites at 353 K

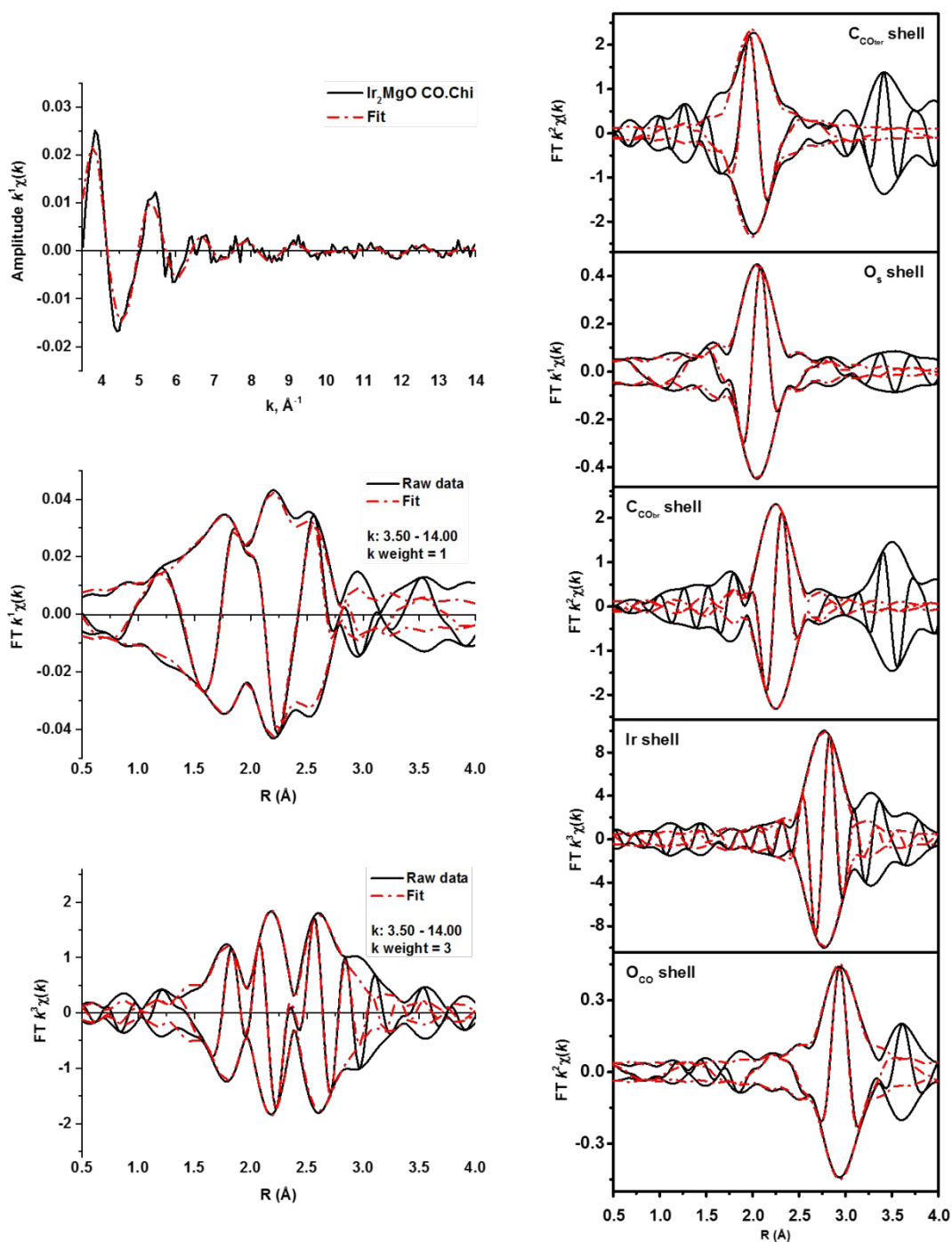


**Supporting Figure S9.** EXAFS characterizing Ir<sub>2</sub>/MgO treated by CO for 1 h at 298 K:  $k^1$ -weighted EXAFS function,  $k^1(\chi)$  (solid line) and sum of the calculated contributions (dashed line);  $k^1$ -weighted and  $k^3$ -weighted and single shell imaginary part and magnitude of the Fourier transform of the data (solid line) and sum of the calculated contributions (dashed line) of the samples.

(A) CO treated Ir pair-sites at 353 K (Model 1)



(B) CO treated Ir pair-sites at 353 K (Model 2)



**Supporting Figure S10.** EXAFS (A) model 1 and (B) model 2 characterizing Ir<sub>2</sub>/MgO treated by CO for 1 h at 353 K:  $k^1$ -weighted EXAFS function,  $k^1(\chi)$  (solid line) and sum of the calculated contributions (dashed line);  $k^1$ -weighted and  $k^3$ -weighted and single shell imaginary part and magnitude of the Fourier transform of the data (solid line) and sum of the calculated contributions (dashed line) of the samples.

**Supporting Table S4.** Summary of Calculated C–O stretching frequencies at the  $\omega$ B97xD//DZVP2(C,O)/cc-pVDZ(Mg)/cc-pVDZ-PP(Ir) for  $\text{Ir}_2(\text{CO})_6$  on MgO and Experiment in  $\text{cm}^{-1}$  with Calculated IR Intensities in  $\text{km/mol}$  in parentheses.

Assignment	$\text{Ir}_2(\text{CO})_6(\text{MgO})_{16}$	$\text{Ir}_2(\text{CO})_6(\text{MgO})_{25}^{\text{a,b}}$	Scaled(0.954)	Experiment
$\nu(\text{CO})$ bridging	1826(684)/	1832(87)	1748	1842
$\nu(\text{CO})$ bridging	1937(654)	1932(658)	1843	1885
$\nu(\text{CO})$ terminal	2101(40)	2094(31)	1998	1953
$\nu(\text{CO})$ terminal	2113(1706)	2106(1782)	2009	1963
$\nu(\text{CO})$ terminal	2140(1687)	2134(1651)	2036	2026
$\nu(\text{CO})$ terminal	2169(598)	2164(511)	2064	2059

<sup>a</sup> Structure (b)

<sup>b</sup>  $\text{Ir}_2(\text{CO})_6(\text{MgO})_{25}$  (a) has CO stretches at 2067(9), 2088(350), 2109(1361), 2114(1264), 2152(1591), and 2194(496)  $\text{cm}^{-1}$  with no stretches.

The calculated values for the CO stretches are reasonably well converged for the  $(\text{MgO})_{25}$  cluster as compared to the  $(\text{MgO})_{16}$  cluster showing that the cluster size is not impacting these values in a significant way for a cluster with at least 16 MgO. There is a clear separation between the calculated CO bridge stretches and the terminal CO stretches with 2 of the former and 4 of the latter. Except for the lowest frequency bridge stretch, the calculated values are larger than experiment as expected. The highest frequency bridge CO is calculated to be  $\sim 50 \text{ cm}^{-1}$  too high. For the terminal stretches, the two lower frequency bands are calculated to be  $\sim 140 \text{ cm}^{-1}$  too high and the two higher frequency bands are predicted to be  $\sim 105 \text{ cm}^{-1}$  too high. We can use the experimental bands for  $\text{C}_{2v} \text{Ir}_2(\text{CO})_8$  with experimental bridging bands of 1822 and 1845  $\text{cm}^{-1}$  and terminal bands of 2060 and 2095  $\text{cm}^{-1}$  as benchmark.<sup>14</sup> The calculated bridging bands (IR intensities in  $\text{km/mol}$  in parentheses) are 1915 (1007) and 1930 (451)  $\text{cm}^{-1}$  and the terminal bands are 2149 (0.0), 2151 (34), 2159 (1761), 2162 (2067), 2190 (1661), and 2227 (28)  $\text{cm}^{-1}$ . This results in a scale factor of 0.954. Use of the scale factor shows that the bridging bands are underestimated and that the lower frequency terminal bands are overestimated by the calculations. The scaled higher energy bands are in excellent agreement with experiment. We note that the CO stretches are very sensitive to the functional.<sup>15</sup>

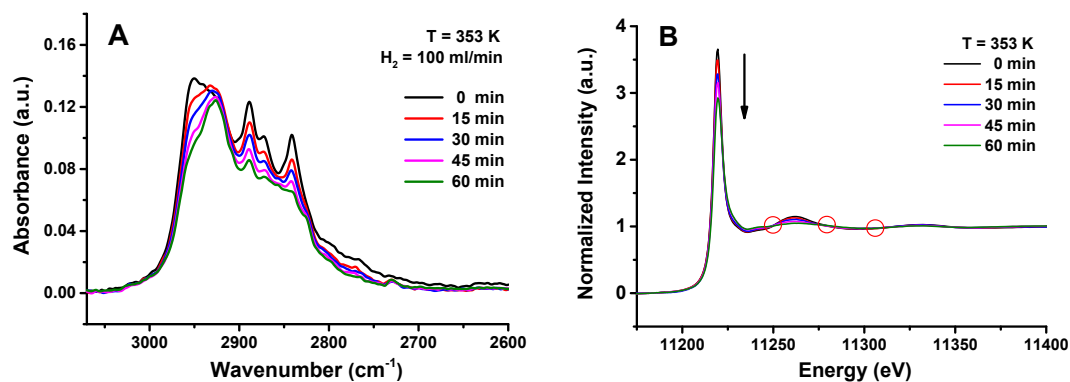
**Supporting Table S5.** CCSD(T)/aD energies in kcal/mol

Reaction	$\Delta H(298K)$	$\Delta G(298K)$
$\text{Ir}_2(\text{CO})_6 \rightarrow 2 \text{Ir}(\text{CO})_3$	59.9	45.1
$\text{Ir}_2(\text{CO})_6 + 2 \text{CO} \rightarrow 2 \text{Ir}(\text{CO})_4$	6.3	13.2
$\text{Ir}_2(\text{CO})_6 + 2 \text{CO} \rightarrow \text{Ir}_2(\text{CO})_8$	-45.1	-23.5

Note: Building on prior work,<sup>15</sup> we have calculated the stability of bare  $\text{Ir}_2(\text{CO})_6$  at the coupled cluster CCSD(T) level using DFT geometries and thermal corrections. The results show that  $\text{Ir}_2(\text{CO})_6$  is stable with respect dissociation to  $\text{Ir}(\text{CO})_3$  and  $\text{Ir}(\text{CO})_4$  (with additional CO). The addition of CO to bare  $\text{Ir}_2(\text{CO})_6$  leads to the exothermic formation of bare  $\text{Ir}_2(\text{CO})_8$ , but we did not predict the formation of  $\text{Ir}_2(\text{CO})_8$  on the MgO surface. Note that many different configurations were studied for the bond of the  $\text{Ir}_2(\text{CO})_x$  clusters to the MgO surface and we show only the ones with actual real binding configurations.

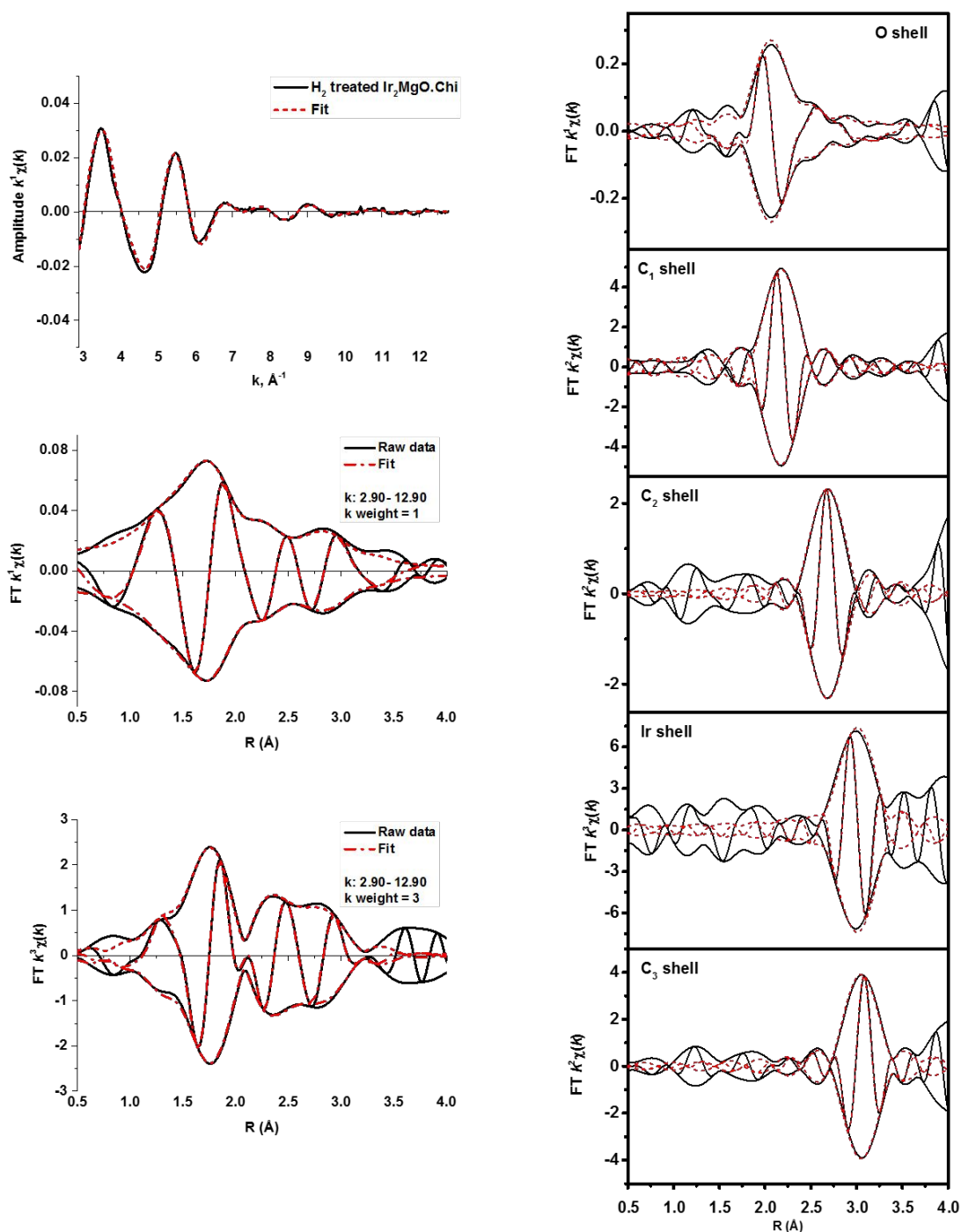


## Reactivity of Iridium Pair-sites towards H<sub>2</sub>

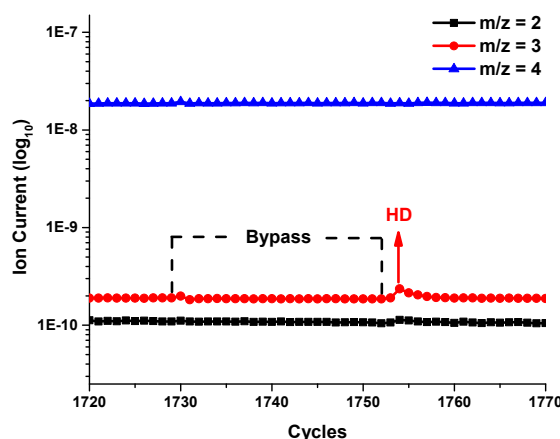


**Supporting Figure S11.** (A) IR spectra in the ν<sub>C-H</sub> region and (B) XANES near the Ir L<sub>III</sub> edge characterizing the sample formed from Ir<sub>2</sub>(μ-OMe)<sub>2</sub>(COD)<sub>2</sub> on MgO showing changes taking place in an atmosphere of H<sub>2</sub> at 353 K and 1 bar. Isosbestic points are circled in red.

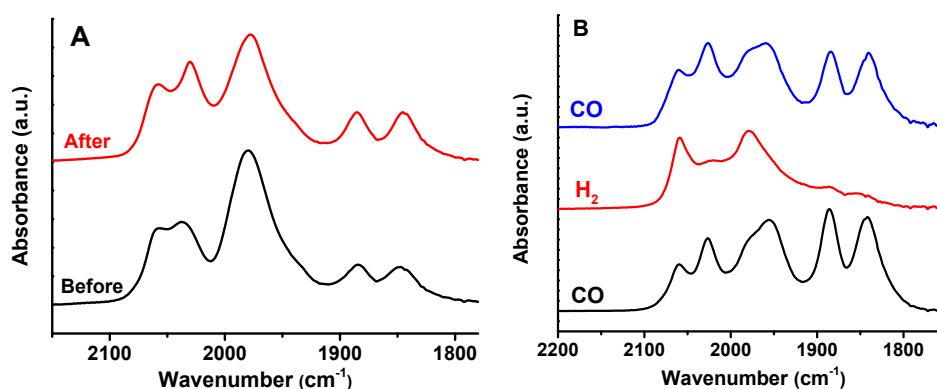
## H<sub>2</sub> treated Ir pair-sites at 353 K



**Supporting Figure S12.** EXAFS model characterizing Ir<sub>2</sub>/MgO treated by H<sub>2</sub> for 1 h at 353 K:  $k^1$ -weighted EXAFS function,  $k^1(\chi)$  (solid line) and sum of the calculated contributions (dashed line);  $k^1$ -weighted and  $k^3$ -weighted and single shell imaginary part and magnitude of the Fourier transform of the data (solid line) and sum of the calculated contributions (dashed line) of the samples.

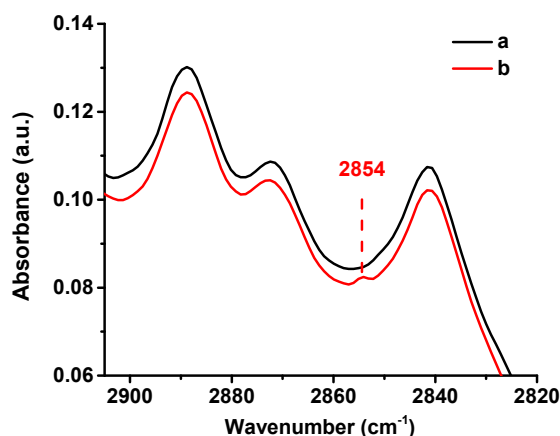


**Supporting Figure S13.** Mass spectra characterizing effluent gas from the IR cell initially containing sample made by adsorption of  $\text{Ir}_2(\mu\text{-OMe})_2(\text{COD})_2$  on MgO after treatment in  $\text{H}_2$  for 1 h at 353 K, then cooled to 298 K and was exposed to  $\text{D}_2$  stream. Before subsequent exposure of the sample to  $\text{D}_2$  (flowing at 20 mL(NTP)/min, balanced with helium flowing at 80 mL(NTP)/min), the residual  $\text{H}_2$  gas was totally purged out by flowing helium. For comparison, we bypassed the cell containing the sample, allowing the gas to flow directly to the mass spectrometer for 3 min, and then switching the gas back through the sample cell; thereupon, an HD pulse ( $M/z = 3$ ) and a slight  $\text{H}_2$  pulse ( $M/z = 2$ ) was detected, confirming the presence of hydride ligands in the sample.

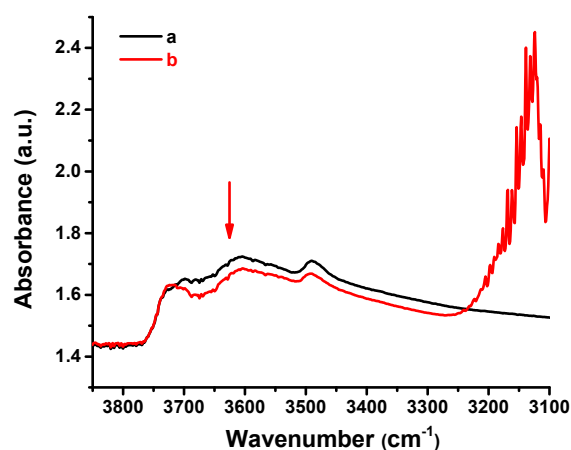


**Supporting Figure S14.** (A) The IR spectra characterizing in the  $\nu_{\text{CO}}$  region of  $\text{Ir}_2/\text{MgO}$  and  $\text{Ir}_2/\text{MgO}$  after treated with flowing  $\text{H}_2$  ( $\text{H}_2$  flow rate = 50 mL(NTP)/min) at 353 K for 1 h; exposure to a 3-min CO pulse, then a purge with He. (B) IR spectra characterizing in the  $\nu_{\text{CO}}$  region of  $\text{Ir}_2/\text{MgO}$  at 353 K and 1 bar exposed to (a) flowing CO (10% CO balanced with He, 50 mL(NTP)/min) for 1 h and then purged with He; (b) aforementioned sample exposed to flowing  $\text{H}_2$  (100 mL(NTP)/min) until bridging CO bands were removed; (c) aforementioned sample exposed to flowing CO (10% CO balanced with He, 50 mL(NTP)/min) and then purge with helium. The exchange of bridging CO ligands with  $\text{H}_2$  is reversible.

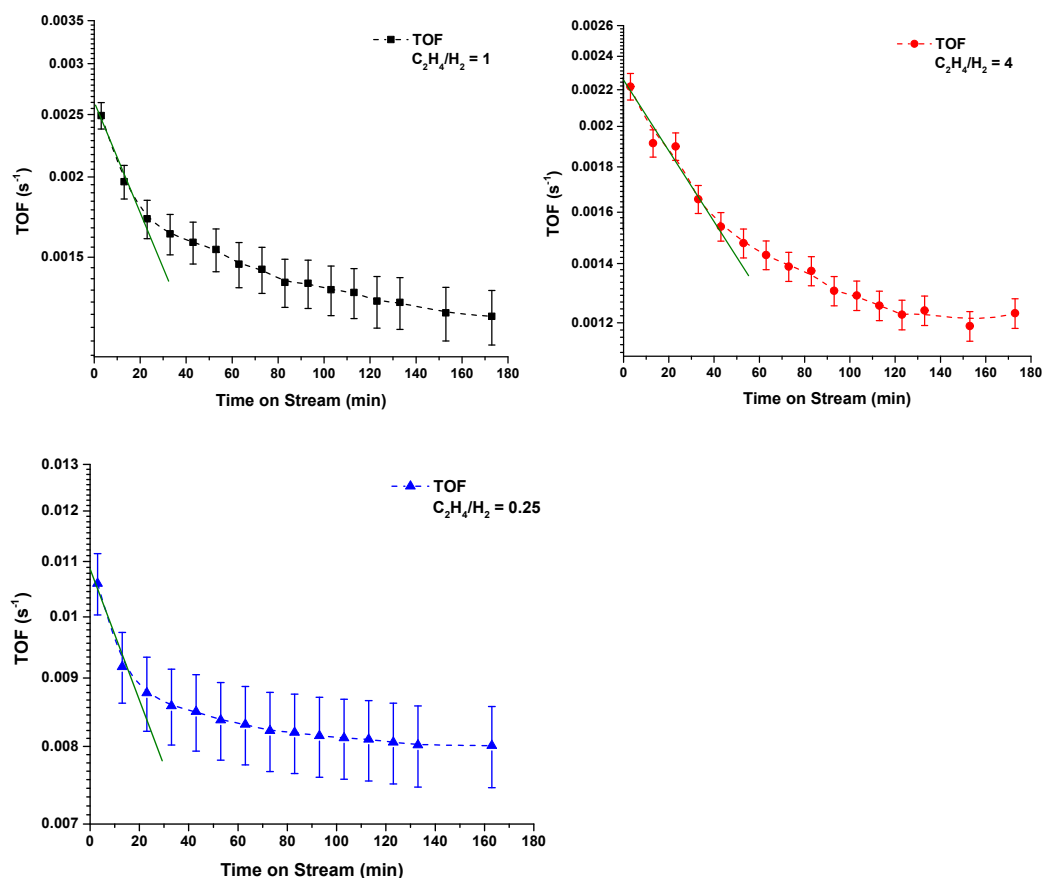
## Structures and Activity of Iridium Pair-sites during Ethylene Hydrogenation



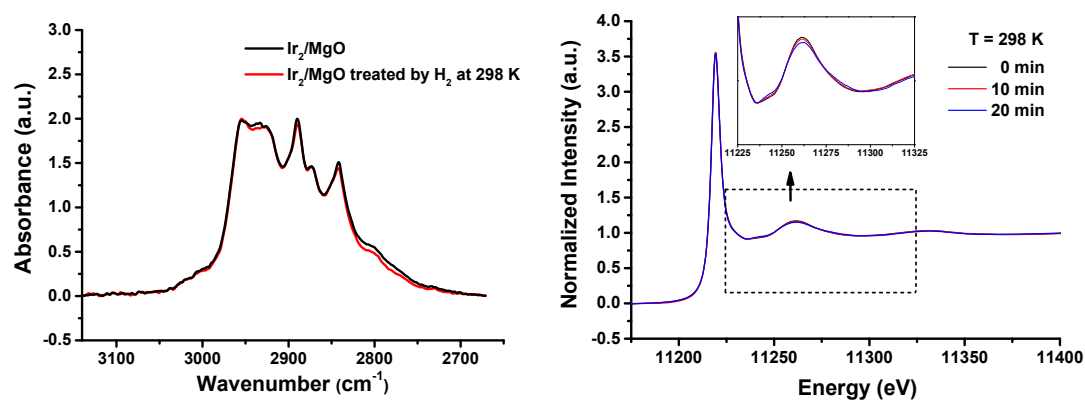
**Supporting Figure S15.** *In-situ* IR spectrum characterizing  $\nu_{\text{CH}}$  of Ir pair sites (a) before and (b) after exposed to flowing  $\text{C}_2\text{H}_4$  at 298 K and 1 bar (flow rate of  $\text{C}_2\text{H}_4 = 50 \text{ mL(NTP)/min}$ ). The IR shoulder at  $2854 \text{ cm}^{-1}$  corresponds to C–H stretch of ethyl groups on Ir.



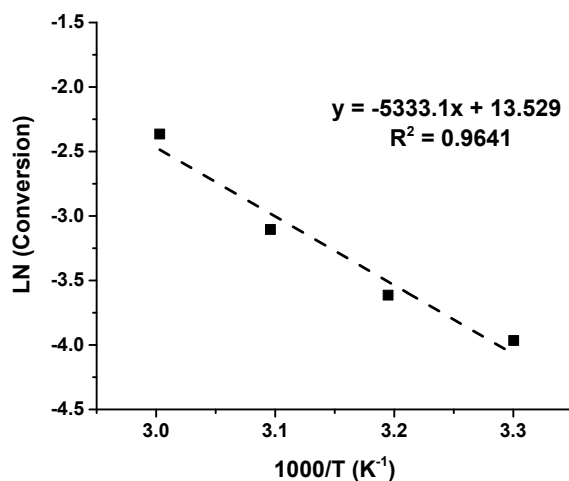
**Supporting Figure S16.** *In-situ* IR spectrum characterizing Ir pair sites (a) before and (b) after exposed to flowing  $\text{C}_2\text{H}_4$  at 298 K and 1 bar (flow rate of  $\text{C}_2\text{H}_4 = 50 \text{ mL(NTP)/min}$ ) for 40 min. The bands characterizing surface -OH groups decreased as time on stream increased. In Figure S17(b), the strong band near  $3150 \text{ cm}^{-1}$  is assigned to the C-H vibrations of gas-phase ethylene (NIST Standard Reference Database of ethylene).



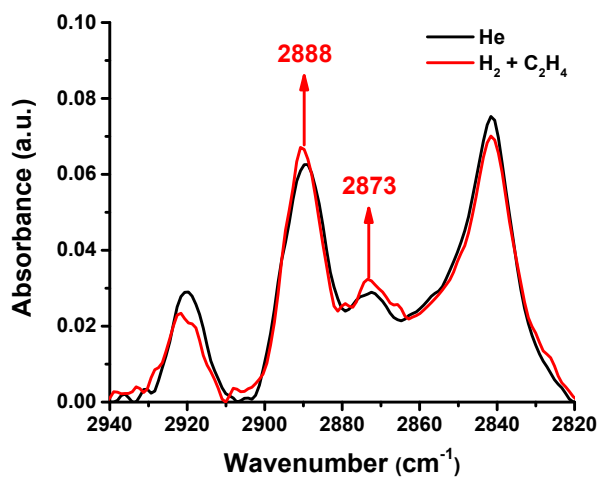
**Supporting Figure S17.** TOF of  $\text{Ir}_2/\text{MgO}$  for ethylene hydrogenation in a flow reactor at 300 K and 1 bar for various feed compositions ( $\text{C}_2\text{H}_4:\text{H}_2$  ratios of 1, 0.25, and 4) for 160 min.



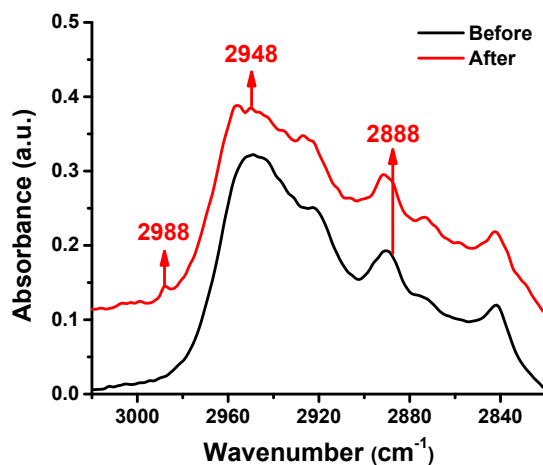
**Supporting Figure S18.**  $\text{Ir}_2/\text{MgO}$  was treated by  $\text{H}_2$  flow ( $\text{H}_2 = 50 \text{ mL/min}$ ) at 298 K. The IR spectra characterizing in the  $\nu_{\text{CH}}$  region and XANES measured at Ir  $\text{L}_{\text{III}}$  edge showed minor changes.



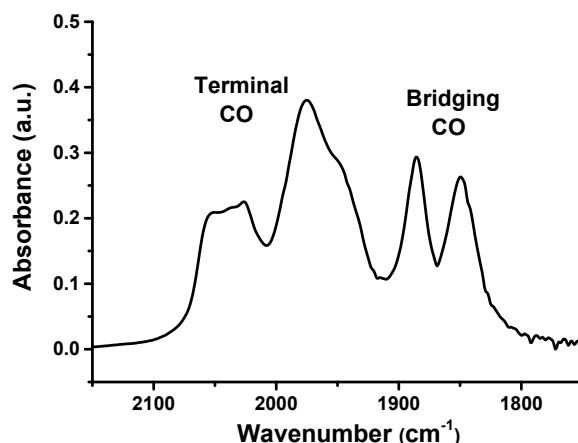
**Supporting Figure S19.** Arrhenius plot for ethylene hydrogenation catalyzed by Ir<sub>2</sub>/MgO at 303–333 K and 1 bar with feed composition of C<sub>2</sub>H<sub>4</sub>:H<sub>2</sub> ratio of 1.0.



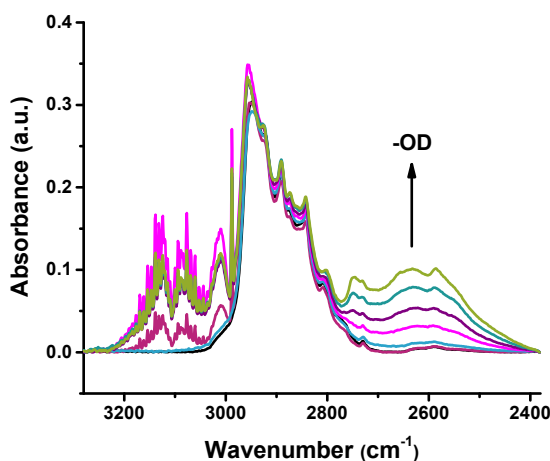
**Supporting Figure S20.** IR spectra in the  $\nu_{\text{C-H}}$  region of the sample formed from Ir<sub>2</sub>( $\mu$ -OMe)<sub>2</sub>(COD)<sub>2</sub> on MgO in He (He = 50 mL/min) and in ethylene hydrogenation condition (C<sub>2</sub>H<sub>4</sub> = H<sub>2</sub> = 20 mL/min, He = 60 mL/min) at 298 K.



**Supporting Figure S21.** Difference in IR spectra in the  $\nu_{\text{C-H}}$  region of the sample formed from  $\text{Ir}_2(\mu\text{-OMe})_2(\text{COD})_2$  on MgO after ethylene hydrogenation condition ( $\text{C}_2\text{H}_4 = \text{H}_2 = 20$  mL/min, He = 60 mL/min) at 298 K for 3 hours, then purged with He (He = 50 mL/min) and initial spectrum of  $\text{Ir}_2(\mu\text{-OMe})_2(\text{COD})_2$  on MgO under He (He = 50 mL/min).



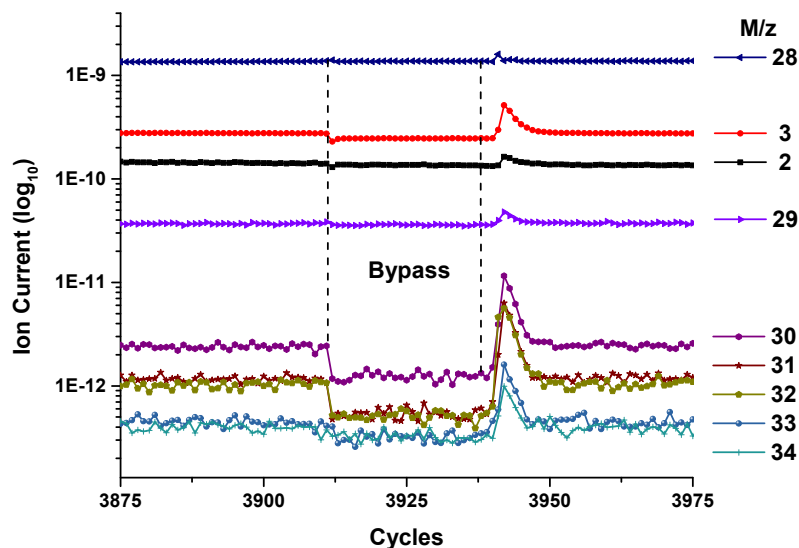
**Supporting Figure S22.** IR spectra characterizing the  $\nu_{\text{CO}}$  region of used MgO-supported iridium pair-site catalyst after ethylene hydrogenation for 3 h, followed by a CO pulse for 3 min (10% CO balanced with helium, 50 mL(NTP)/min) and purged with helium. The positions of the  $\nu_{\text{CO}}$  bands are the same as those characterizing the initial  $\text{Ir}_2/\text{MgO}$  catalyst that had been exposed to CO, showing that the pair-site structure was retained during catalysis.



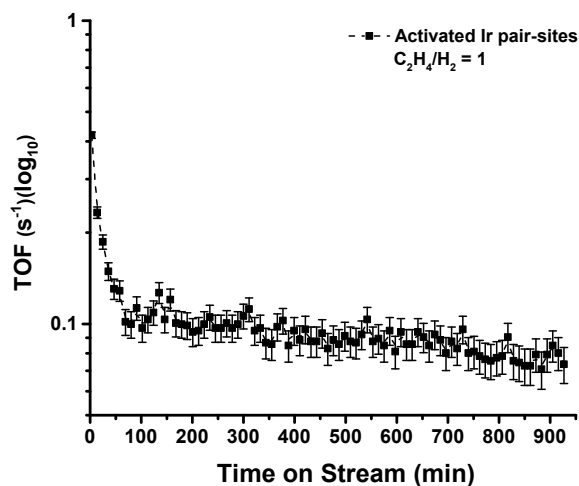
**Supporting Figure S23.** IR spectra in  $\nu_{\text{C-H}}$  ( $\nu_{\text{O-D}}$ ) region characterizing the sample formed from  $\text{Ir}_2(\mu\text{-OMe})_2(\text{COD})_2$  on MgO in flowing gases: flow rates:  $\text{C}_2\text{H}_4 = \text{D}_2 = 20$  mL(NTP)/min at 298 K and 1 bar.

Note: Regarding the hydrogen spillover to MgO, we flowed  $\text{D}_2/\text{He}$  (flow rates:  $\text{D}_2 = 15$ , He = 50 mL(NTP)/min) to the MgO support without iridium at room temperature and did not observe significant hydrogen spillover, as indicated by IR spectroscopy showing a lack of change in the intensities of OH and OD groups. Consistent with these

observations, we found no evidence from the analysis by mass spectrometry of the effluent gas that HD had formed. These observations excludes the occurrence of HD exchange happens on the OH groups on MgO.



**Supporting Figure S24.** Mass spectra characterizing effluent gas from the IR cell initially containing sample made by adsorption of  $\text{Ir}_2(\mu\text{-OMe})_2(\text{COD})_2$  on MgO under conditions of ethylene deuterium-hydrogenation (flow rates:  $\text{C}_2\text{H}_4 = \text{D}_2 = 20$  mL(NTP)/min, He = 60 mL(NTP)/min) at 298 K and 1 bar. (The ion current of  $m/z$  from 31 to 34 was not observed in ethylene hydrogenation without  $\text{D}_2$ .)

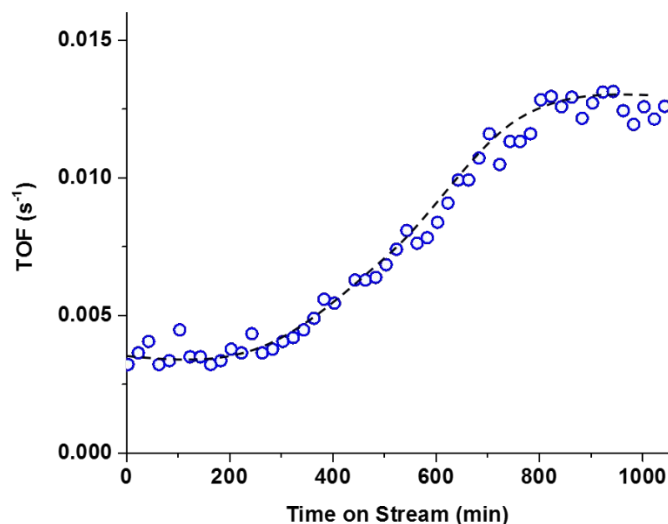


**Supporting Figure S25.** TOF of  $\text{Ir}_2/\text{MgO}$  after activation under  $\text{H}_2$  flow (50 mL/min, NTP) at 353 K for 1 h, then cooling to 300 K in He. Ethylene hydrogenation was test in a flow reactor at 300 K and 1 bar with  $\text{C}_2\text{H}_4:\text{H}_2$  ratios of 1.

Note: The modified catalyst lost 80% of its initial activity after 1 h, and then showed

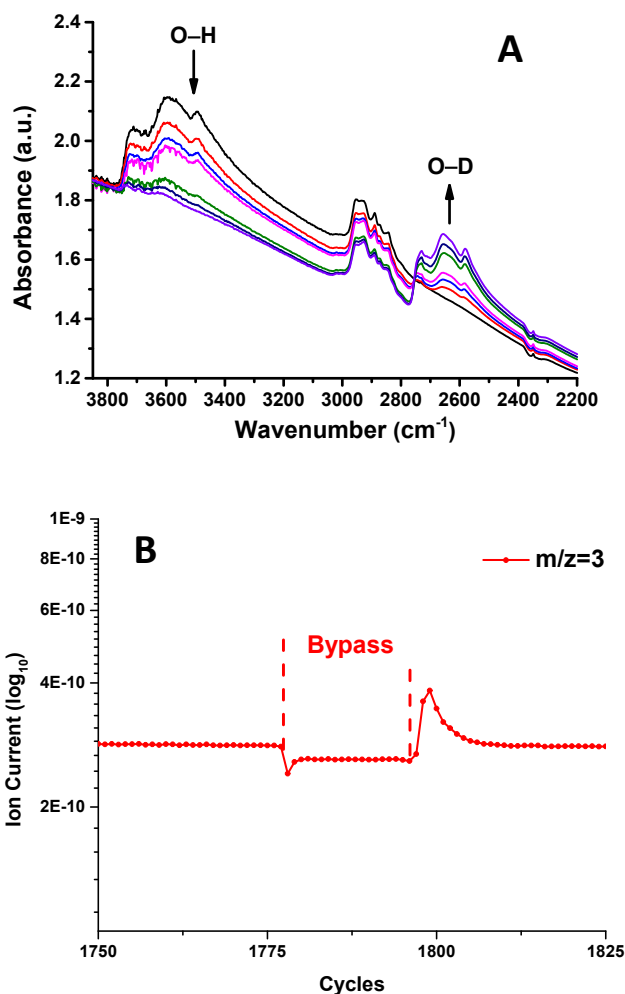


no deactivation for at least 18 h. The changes in the ligands on the iridium resulting from the H<sub>2</sub> treatment led to an increased catalytic activity of the iridium pair-sites.



**Supporting Figure S26.** Increasing activity of the supported iridium pair-site catalyst that was initially poisoned with CO as CO desorbed during catalytic reaction. The feed component flow rates of C<sub>2</sub>H<sub>4</sub> and of H<sub>2</sub> were 20 mL(NTP)/min and that of helium was 60 mL(NTP)/min; the temperature was 298 K and the pressure 1.0 bar. The catalyst had been pretreated by exposure to flowing CO flow for 1 h at 298 K and 1.0 bar.

Note: The data showed the advantage of pair-site catalysts that contain bridging bonding sites. The single-site iridium catalysts on MgO with initial form of Ir(C<sub>2</sub>H<sub>4</sub>)<sub>2</sub>/MgO under CO treatment are fully deactivated as iridium gem-dicarbonyls (Ir(CO)<sub>2</sub>/MgO) form when CO is present. Group-8 metal carbonyl complexes are usually more stable than their ethylene complexes<sup>15</sup> and when the metal is supported on the electron donating support, such as MgO, the metal carbonyl complexes are so stable that replacement of the CO ligands by C<sub>2</sub>H<sub>4</sub> do not occur under C<sub>2</sub>H<sub>4</sub> flow at room temperature.<sup>16</sup>



**Supporting Figure S27.** (A) IR spectrum characterizing iridium pair sites doing H-D exchange in the presence of flowing  $\text{H}_2 + \text{D}_2$  at 353 K and 1 bar (flow rates of  $\text{H}_2$  and of  $\text{D}_2$ , each 20 mL(NTP)/min). Formation of OD groups on the support is inferred to have taken place by spillover of D. (B) Mass spectrum characterizing HD exchange as IR data was being recorded; experiments with reactant flowing through a bypass of the reactor were conducted for a comparison that confirmed the dissociation of  $\text{H}_2$  and  $\text{D}_2$  and the catalytic reaction took place only on the catalyst.

**Additional Information for DFT Models**

**Supporting Table S6.** Optimized x,y,z coordinates in Angstroms at  $\omega$ B97xD//DZVP2(C,O)/cc-pVDZ(Mg)/cc-pVDZ-PP(Ir)

**Ir<sub>2</sub>(COD)<sub>2</sub>(CH<sub>3</sub>O)<sub>2</sub>**

0 1

C	3.075162	-1.317542	-0.426406
H	2.896753	-2.009058	-1.248710
C	2.321804	-1.540611	0.767825
H	1.628763	-2.382133	0.754645
C	3.077159	1.407019	-0.115660
H	2.811636	2.355338	-0.582596
C	2.530828	1.155198	1.180657
H	1.879124	1.926046	1.589434
C	4.391035	0.833994	-0.619220
H	5.241470	1.337352	-0.142736
H	4.453185	1.055897	-1.687841
C	3.245944	0.306939	2.230373
H	3.044367	0.712983	3.223717
H	4.327166	0.377275	2.086425
C	2.779759	-1.157981	2.164302
H	1.924476	-1.290924	2.832464
H	3.565158	-1.838292	2.516170
C	4.468146	-0.690071	-0.417014
H	4.973989	-0.932177	0.521367
H	5.071356	-1.135498	-1.210581
C	-3.077587	1.406600	-0.116605
H	-2.812308	2.354655	-0.584226
C	-2.531257	1.155873	1.179924
H	-1.879858	1.927242	1.588205
C	-3.074695	-1.318136	-0.425623
H	-2.896022	-2.010192	-1.247418
C	-2.321348	-1.540137	0.768820
H	-1.627984	-2.381407	0.756249
C	-4.467891	-0.691125	-0.416730
H	-4.973732	-0.932801	0.521765
H	-5.070900	-1.137242	-1.210062
C	-2.779521	-1.156756	2.165024
H	-1.924240	-1.289010	2.833326
H	-3.564734	-1.837088	2.517263
C	-3.246155	0.308065	2.230145
H	-3.044738	0.714793	3.223242
H	-4.327396	0.377979	2.086122
C	-4.391254	0.832838	-0.619877

H	-5.241861	1.336236	-0.143742
H	-4.453425	1.054057	-1.688638
IR	-1.500711	0.057236	-0.273432
IR	1.500717	0.057207	-0.273464
O	0.000002	-1.034301	-1.213136
O	-0.000012	1.445501	-0.723612
C	-0.000023	2.807712	-0.355795
H	0.001016	2.944073	0.733003
H	0.883940	3.303288	-0.768320
H	-0.885076	3.302850	-0.766502
C	-0.000113	-2.411020	-1.517555
H	-0.001176	-3.039408	-0.617600
H	-0.886544	-2.655530	-2.110312
H	0.887264	-2.656131	-2.108635

**Ir<sub>2</sub>(COD)<sub>2</sub>(MgO)<sub>25</sub> (Ir top O)**

0 1

O	-2.967441	-1.834866	1.724264
O	0.219915	-0.186802	3.368146
MG	-3.462352	-0.111369	0.838812
O	-1.820129	0.703318	1.687358
MG	-0.212149	1.568679	2.549166
O	-3.933067	1.650664	0.050113
MG	-2.308981	2.492685	0.846657
O	-0.741607	3.304885	1.742794
MG	-1.822632	-2.401718	-0.034694
O	-0.026196	-1.644514	0.558054
MG	1.591347	-0.757843	1.526519
O	-2.291973	-0.645376	-0.898973
O	0.991798	1.038338	0.725719
MG	-2.737808	1.130183	-1.743699
O	-1.110488	1.984662	-0.917280
MG	0.535180	2.836677	-0.075975
MG	-1.409654	-1.005649	2.639433
MG	-2.499732	-3.628872	2.556865
O	-0.880224	-2.824497	3.414328
MG	0.742735	-1.953159	4.198913
O	-1.352044	-4.200571	0.927456
MG	0.260946	-3.334823	1.753110
O	1.899786	-2.544356	2.561908
MG	-4.386801	3.413116	-0.845340
O	-2.824403	4.318161	-0.005647
MG	-1.201636	5.081634	0.867916
O	-3.225521	2.966699	-2.583665

MG	-1.667637	3.798022	-1.642774
O	-0.043734	4.665144	-0.870497
O	1.420486	2.430560	3.439141
MG	0.894972	4.162309	2.581625
O	3.098333	0.209041	2.576106
MG	2.566079	1.963759	1.761650
O	2.112804	3.730983	0.965956
MG	1.867697	0.652767	4.208595
O	2.298972	-1.089460	5.054572
MG	3.297651	-1.514598	3.472855
O	0.362811	5.898608	1.756838
MG	1.404134	5.385426	0.229327
O	-5.150673	-0.976876	-0.005354
MG	-5.538556	0.797030	-0.848164
O	-3.510089	-3.242187	-0.885708
MG	-3.986724	-1.460635	-1.652949
O	-4.423074	0.244413	-2.587146
MG	-4.612856	-2.692815	0.851462
O	-4.130588	-4.401127	1.723380
MG	-3.054167	-4.806928	0.184846
O	-5.971118	2.546489	-1.670181
MG	-4.856472	2.064312	-3.154759
MG	-0.688091	0.218022	-0.044890
C	2.573375	2.518891	-1.912611
H	1.726598	3.208995	-1.921263
C	2.479912	1.443016	-2.853463
H	1.484981	1.305365	-3.288920
C	4.360635	0.947474	-0.460035
H	4.605403	0.505810	0.508663
C	4.387400	0.042708	-1.591926
H	4.709359	-0.968315	-1.364851
C	4.747284	2.416911	-0.580394
H	5.821231	2.494028	-0.795499
H	4.599493	2.910818	0.386328
C	4.824047	0.529458	-2.976948
H	5.316606	-0.285635	-3.511622
H	5.571651	1.322514	-2.876481
C	3.611058	1.022681	-3.778671
H	3.241231	0.216474	-4.417777
H	3.878131	1.850266	-4.447280
C	3.915652	3.182108	-1.630411
H	4.484276	3.285755	-2.561476
H	3.748735	4.196747	-1.259205
C	3.128581	-3.098923	-1.735212

H	4.004007	-2.739353	-1.197686
C	2.625383	-2.265766	-2.768398
H	3.159911	-1.345544	-2.931991
C	0.521552	-4.057243	-1.563032
H	-0.100841	-4.405283	-0.742207
C	0.003506	-3.001316	-2.340753
H	-1.008774	-2.650845	-2.126343
C	1.553325	-5.061198	-2.044476
H	1.452420	-5.229819	-3.118592
H	1.357354	-6.025003	-1.567967
C	0.369522	-2.722099	-3.783026
H	-0.002899	-1.722629	-4.027517
H	-0.145687	-3.425033	-4.449818
C	1.887337	-2.758733	-4.005077
H	2.143277	-2.112524	-4.848618
H	2.221016	-3.760992	-4.282317
C	2.981654	-4.605548	-1.695090
H	3.716401	-5.077460	-2.359927
H	3.222438	-4.934680	-0.679214
IR	1.446541	-2.095632	-1.009439
IR	2.428500	0.493381	-1.002364

# $\text{Ir}_2(\text{COD})_2(\text{MgO})_{25}$

0 1

O	-2.758140	0.943502	-2.518401
O	0.106778	3.484788	-1.602364
MG	-1.439646	-0.516392	-2.841600
O	0.037086	0.807990	-2.438443
MG	1.517043	2.113642	-1.980395
O	-0.031206	-1.858241	-3.299313
MG	1.416197	-0.522649	-3.074768
O	2.834388	0.752122	-2.590215
MG	-2.869392	0.171803	-0.258063
O	-1.358865	1.386719	0.498710
MG	0.130345	2.776175	0.600907
O	-1.472953	-1.141813	-0.878203
O	1.511318	1.492387	-0.024896
MG	-0.098638	-2.557130	-1.111368
O	1.389261	-1.386972	-0.363753
MG	2.888729	0.031814	-0.160654
MG	-1.333506	2.270182	-2.199204
MG	-4.157049	2.300297	-1.979883
O	-2.721388	3.618080	-1.516560
MG	-1.251162	4.868293	-1.039889

O	-4.244471	1.715427	-0.000492
MG	-2.734758	2.926146	0.452337
O	-1.312830	4.221503	0.970590
MG	1.321088	-3.317746	-3.630994
O	2.793803	-2.026551	-3.276795
MG	4.225822	-0.684013	-2.853949
O	1.345653	-3.963341	-1.620612
MG	2.768866	-2.611404	-1.277459
O	4.268356	-1.366245	-0.898455
O	3.028145	3.500322	-1.574848
MG	4.312867	2.030921	-2.030706
O	1.645414	4.150766	0.962023
MG	2.993137	2.817297	0.367911
O	4.376841	1.439787	0.029508
MG	1.589976	4.791175	-1.090152
O	0.208991	6.133544	-0.623634
MG	0.205117	5.437429	1.164419
O	5.655611	0.638587	-2.467801
MG	5.573146	0.067274	-0.646815
O	-2.947349	-1.860870	-3.349562
MG	-1.519359	-3.208916	-3.673261
O	-4.356949	-1.114963	-0.894908
MG	-2.963915	-2.436221	-1.362441
O	-1.616940	-3.876212	-1.630403
MG	-4.246550	-0.404057	-2.890895
O	-5.579105	1.004306	-2.474793
MG	-5.545395	0.412064	-0.654362
O	-0.143197	-4.579986	-4.051538
MG	-0.175243	-5.053384	-2.192260
MG	0.022324	0.156343	-0.392563
C	3.472877	-1.496298	2.106861
H	3.985918	-1.748768	1.182054
C	2.583089	-2.488272	2.605528
H	2.465024	-3.379135	1.981993
C	1.906497	0.518798	3.190362
H	1.342034	1.433921	3.000289
C	1.230431	-0.490811	3.939546
H	0.232028	-0.235388	4.272412
C	3.403918	0.750316	3.275856
H	3.655407	1.189817	4.249634
H	3.694390	1.484270	2.518417
C	1.971125	-1.470849	4.843611
H	1.339045	-1.730137	5.696242
H	2.859164	-0.994061	5.267808

C	2.351858	-2.752953	4.083691
H	1.537505	-3.477514	4.174638
H	3.238613	-3.222905	4.527464
C	4.222312	-0.527944	3.010481
H	4.499063	-1.014392	3.950232
H	5.164128	-0.240116	2.531889
C	-3.454080	0.175113	2.582817
H	-3.828143	1.100761	2.152957
C	-2.518913	0.276879	3.659515
H	-2.199529	1.286717	3.923810
C	-2.255640	-2.247748	2.128841
H	-1.944365	-2.831950	1.259589
C	-1.276687	-2.134974	3.169865
H	-0.365980	-2.715155	3.051156
C	-3.752650	-2.343970	2.434894
H	-3.885607	-2.882369	3.379571
H	-4.234569	-2.953103	1.665582
C	-1.683954	-1.951789	4.620639
H	-0.776058	-1.882056	5.220999
H	-2.209537	-2.846495	4.977470
C	-2.550873	-0.694364	4.842446
H	-2.215316	-0.172545	5.741079
H	-3.590117	-0.983435	5.030167
C	-4.446163	-0.970460	2.497926
H	-5.162418	-0.939380	3.329372
H	-5.030848	-0.852602	1.579780
IR	-1.398247	-0.370457	2.013430
IR	1.312334	-0.973990	1.876605

**Ir<sub>2</sub>O<sub>2</sub>(COD)<sub>2</sub>(MgO)<sub>25</sub><sup>-2</sup>**

-2 1

O	-3.505025	1.393437	1.511759
O	-0.308575	0.817044	3.896205
Mg	-2.406241	2.614759	0.370277
O	-0.833746	2.345786	1.523688
Mg	0.799489	1.868297	2.586522
O	-1.384807	3.983724	-0.717589
Mg	0.259236	3.532229	0.384075
O	1.841891	3.308138	1.577602
Mg	-2.845142	-0.347005	0.037068
O	-1.319604	-0.595077	1.271103
Mg	0.474023	-1.415676	1.904496
O	-1.930064	1.082747	-1.010970
O	1.366809	0.347672	1.289441



MG	-0.783326	2.250675	-2.120774
O	0.824620	2.042145	-0.982395
MG	2.446165	1.392797	-0.008734
MG	-1.810974	0.947347	2.576722
MG	-4.480693	-0.023316	2.528497
O	-2.968248	-0.467733	3.727417
MG	-1.232954	-0.763728	4.680331
O	-4.005896	-1.623136	1.237341
MG	-2.354480	-1.892667	2.352752
O	-0.765616	-2.415787	3.387973
MG	-0.295721	5.197960	-1.856451
O	1.378553	4.969952	-0.812477
MG	2.919647	4.436803	0.358049
O	0.295837	3.685389	-3.261274
MG	1.848705	3.373363	-2.030544
O	3.519385	2.936276	-1.062058
O	2.575971	1.457917	3.748545
MG	3.485056	2.746388	2.544359
O	2.055023	-1.436286	3.401506
MG	2.976895	-0.036621	2.377515
O	4.110031	1.178319	1.255358
MG	1.389152	0.148984	4.688683
O	0.383851	-1.199864	5.798299
MG	0.833534	-2.479047	4.446470
O	4.570228	4.064199	1.443795
MG	4.900278	2.607362	0.241860
O	-4.167846	3.064639	-0.802903
MG	-2.987243	4.278084	-1.857429
O	-4.628845	0.154745	-1.074847
MG	-3.563225	1.520634	-2.039340
O	-2.537660	2.729080	-3.260265
MG	-5.077104	1.684117	0.337866
O	-6.141417	0.372851	1.430310
MG	-5.504740	-0.976545	0.218271
O	-1.932424	5.594029	-2.965861
MG	-1.421869	4.090822	-4.045239
MG	-0.196833	0.520918	-0.011967
C	3.377411	-0.519438	-2.164022
H	3.017966	0.497857	-2.338404
C	2.732703	-1.531089	-2.953664
H	1.888928	-1.194927	-3.556851
C	3.939342	-2.293508	-0.121752
H	3.823019	-2.503849	0.944642
C	3.490094	-3.315617	-1.018045

H	3.015236	-4.186776	-0.568802
C	5.094078	-1.359758	-0.463894
H	6.045273	-1.912611	-0.500159
H	5.167476	-0.622632	0.339861
C	4.152277	-3.550218	-2.375569
H	4.157365	-4.620613	-2.604822
H	5.202757	-3.240958	-2.334959
C	3.411213	-2.783260	-3.487476
H	2.617664	-3.423023	-3.888499
H	4.087263	-2.550126	-4.324155
C	4.859798	-0.597569	-1.787970
H	5.426839	-1.055262	-2.607744
H	5.245797	0.426547	-1.697065
C	-1.647798	-4.221214	-0.197433
H	-1.434649	-4.333840	0.868927
C	-0.661042	-4.742676	-1.095312
H	0.240120	-5.157550	-0.645464
C	-2.265337	-2.438622	-2.211554
H	-2.584249	-1.403115	-2.350244
C	-1.136595	-2.835893	-3.004271
H	-0.667449	-2.046301	-3.591767
C	-3.399643	-3.404590	-1.859883
H	-3.568962	-4.097490	-2.693113
H	-4.326364	-2.823979	-1.761942
C	-0.914269	-4.234139	-3.559741
H	0.104215	-4.254248	-3.962436
H	-1.593392	-4.447728	-4.399220
C	-1.036083	-5.311027	-2.464371
H	-0.385650	-6.158176	-2.704546
H	-2.056811	-5.708592	-2.434029
C	-3.130035	-4.177526	-0.548918
H	-3.548083	-5.194243	-0.607683
H	-3.645331	-3.654548	0.261078
IR	-0.529488	-2.665656	-1.041611
IR	2.115163	-1.750203	-1.001094
O	0.336150	-0.864669	-1.397635
O	0.923645	-2.642915	0.394044

**Ir<sub>2</sub>(OH)<sub>2</sub>(COD)<sub>2</sub>(MgO)<sub>25</sub>**

0 1

O	-2.533750	-2.646666	1.493662
O	-0.184186	-0.182729	3.491736
MG	-3.405842	-1.106844	0.556715
O	-2.203768	0.118997	1.579479

MG	-1.025642	1.390080	2.592685
O	-4.315404	0.452791	-0.283367
MG	-3.097679	1.702468	0.685255
O	-1.979765	2.940533	1.758864
MG	-1.094466	-2.776157	-0.112757
O	0.362373	-1.601055	0.647608
MG	1.408366	-0.239932	1.857980
O	-1.958434	-1.229900	-1.053550
O	0.428659	1.340403	1.059148
MG	-2.840646	0.368503	-1.908911
O	-1.663167	1.654950	-0.921127
MG	-0.447316	2.881697	0.126485
MG	-1.414765	-1.413437	2.575126
MG	-1.644315	-4.242102	2.384806
O	-0.448724	-3.024640	3.415051
MG	0.731629	-1.743335	4.385750
O	-0.211936	-4.420701	0.896780
MG	0.974136	-3.115182	1.874633
O	2.200849	-1.894765	2.897643
MG	-5.176818	2.029421	-1.224890
O	-4.057615	3.342631	-0.228592
MG	-2.835774	4.515360	0.822837
O	-3.758561	1.999029	-2.830613
MG	-2.632386	3.227023	-1.714211
O	-1.398690	4.497790	-0.785304
O	0.144607	2.696820	3.725290
MG	-0.769202	4.201808	2.772769
O	2.521009	1.095442	3.057784
MG	1.530727	2.603110	2.192298
O	0.727325	4.185809	1.272673
MG	1.003473	1.093976	4.539100
O	1.835933	-0.474729	5.429764
MG	3.084987	-0.523499	3.977380
O	-1.670659	5.731523	1.865403
MG	-0.369731	5.575961	0.467279
O	-4.676046	-2.415512	-0.465434
MG	-5.486817	-0.812531	-1.345602
O	-2.343661	-4.069149	-1.151638
MG	-3.250168	-2.480926	-1.967174
O	-4.079461	-0.957862	-2.953881
MG	-3.750937	-3.915323	0.456922
O	-2.890482	-5.434891	1.384802
MG	-1.582518	-5.459703	-0.019141
O	-6.333888	0.753937	-2.217523

MG	-4.970201	0.664101	-3.566220
MG	-0.669565	0.064931	-0.115918
C	1.821280	3.077299	-2.221391
H	0.735163	3.160930	-2.298378
C	2.426823	2.097038	-3.074326
H	1.743754	1.516237	-3.697426
C	3.726240	2.777706	-0.269858
H	3.907697	2.540683	0.782971
C	4.420691	1.958865	-1.213207
H	5.049366	1.163822	-0.808350
C	3.355085	4.226899	-0.540743
H	4.255784	4.851539	-0.579079
H	2.742119	4.567398	0.296441
C	4.872669	2.490336	-2.571801
H	5.829385	2.039400	-2.842261
H	5.050672	3.566334	-2.499297
C	3.826396	2.184179	-3.655987
H	4.048706	1.212257	-4.105739
H	3.866441	2.923960	-4.464542
C	2.525053	4.376497	-1.831626
H	3.147750	4.716306	-2.664672
H	1.764689	5.151445	-1.692662
C	3.934993	-2.751136	-0.804886
H	4.545239	-2.359858	0.013002
C	3.843199	-1.911267	-1.987025
H	4.383039	-0.965242	-1.940889
C	1.560915	-3.760952	-1.579086
H	0.708830	-4.136816	-1.021572
C	1.324125	-2.777990	-2.579040
H	0.285852	-2.469858	-2.721717
C	2.704652	-4.769974	-1.640926
H	2.972436	-4.965794	-2.681964
H	2.358282	-5.720681	-1.228762
C	2.209570	-2.552757	-3.793483
H	1.904397	-1.605864	-4.249819
H	2.037259	-3.332108	-4.545828
C	3.695748	-2.460928	-3.405828
H	4.214083	-1.802302	-4.105865
H	4.184884	-3.434566	-3.490791
C	3.915999	-4.267654	-0.843831
H	4.855164	-4.664211	-1.248905
H	3.842788	-4.624636	0.187787
IR	2.098898	-1.831575	-0.890559
IR	2.418697	1.393043	-1.136474

O	0.836495	0.117857	-1.566793
O	2.807234	-0.193079	0.256945
H	3.729155	-0.253780	0.528558
H	0.528989	0.139106	-2.477206

# $\text{Ir}_2(\text{CO})_6(\text{MgO})_{25}$

0 1

O	1.623064	2.649348	2.016483
O	-1.274592	0.144183	3.104114
Mg	2.775288	1.119232	1.427919
O	1.291503	-0.150445	2.005179
Mg	-0.152824	-1.424908	2.591787
O	3.893312	-0.447985	0.913640
Mg	2.447356	-1.721785	1.420580
O	0.979612	-2.951185	2.006541
Mg	0.787202	2.773081	0.007145
O	-0.728065	1.516476	0.483282
Mg	-2.163146	0.248527	1.107866
O	1.912299	1.219724	-0.570232
O	-1.052958	-1.311247	0.479296
Mg	3.028108	-0.346935	-1.152404
O	1.584145	-1.619477	-0.577794
Mg	0.137133	-2.878441	-0.006239
Mg	0.173125	1.417263	2.596077
Mg	0.465359	4.241020	2.525425
O	-1.015805	3.020449	3.131130
Mg	-2.456608	1.722958	3.628458
O	-0.414209	4.362740	0.606797
Mg	-1.811573	3.103142	1.221988
O	-3.298783	1.872885	1.687466
Mg	5.009358	-2.017702	0.268265
O	3.608929	-3.340136	0.833339
Mg	2.106489	-4.539758	1.375806
O	4.194076	-1.971450	-1.699588
Mg	2.767872	-3.199747	-1.062250
O	1.301958	-4.469878	-0.596632
O	-1.672720	-2.715084	3.128735
Mg	-0.506029	-4.238034	2.518303
O	-3.635825	-1.077568	1.692454
Mg	-2.465518	-2.613153	1.225005
O	-1.394310	-4.154782	0.600958
Mg	-2.781858	-1.119450	3.631205
O	-3.872279	0.446487	4.156127
Mg	-4.543505	0.519912	2.354563

O	0.637988	-5.745328	1.935963
MG	-0.116368	-5.566892	0.176936
O	4.274983	2.434305	0.842565
MG	5.338233	0.826581	0.270746
O	2.284335	4.058719	-0.585357
MG	3.423288	2.488821	-1.052647
O	4.535407	0.972682	-1.693141
MG	3.082278	3.942075	1.385835
O	1.922793	5.449530	1.946919
MG	1.152895	5.447890	0.184551
O	6.424013	-0.739554	-0.281289
MG	5.586857	-0.639766	-2.005448
MG	0.483748	-0.053983	0.023591
IR	-1.572907	1.675023	-1.890739
IR	-1.949188	-1.269337	-1.876127
C	-0.039802	1.390046	-2.984587
O	0.848388	1.360327	-3.723057
C	-3.469634	1.827720	-1.714007
O	-4.602673	2.049868	-1.714356
C	-3.820394	-0.955302	-1.637686
O	-4.972782	-0.894184	-1.600135
C	-0.432898	-1.366736	-3.022487
O	0.410873	-1.555643	-3.789071
C	-1.454854	3.516057	-2.252693
O	-1.399652	4.626243	-2.564685
C	-2.290877	-3.084654	-2.227215
O	-2.512247	-4.175015	-2.535152

**Ir<sub>2</sub>(CO)<sub>4</sub>(CO)<sub>2</sub>(MgO)<sub>25</sub>**

0 1

O	-1.312160	-2.815642	2.010212
O	1.229702	0.000506	3.146134
MG	-2.617033	-1.431585	1.387411
O	-1.285675	-0.003066	1.989268
MG	-0.058530	1.434414	2.669817
O	-3.905447	-0.007691	0.873996
MG	-2.622325	1.420736	1.388348
O	-1.323065	2.808797	2.013161
MG	-0.430315	-2.860508	0.029416
O	0.976295	-1.442437	0.411458
MG	2.186476	0.002571	1.222204
O	-1.723578	-1.436218	-0.567232
O	0.970734	1.444564	0.411511
MG	-3.005265	-0.004979	-1.170422

O	-1.729124	1.430308	-0.565502
MG	-0.440924	2.858006	0.032675
MG	-0.052019	-1.437400	2.666215
MG	0.002566	-4.271113	2.559860
O	1.298705	-2.878352	3.189649
MG	2.590455	-1.435217	3.727899
O	0.925781	-4.297667	0.664083
MG	2.172076	-2.883656	1.289938
O	3.457548	-1.494360	1.854972
MG	-5.190709	1.422965	0.210794
O	-3.965220	2.895672	0.801392
MG	-2.626070	4.259695	1.375576
O	-4.335923	1.475033	-1.743791
MG	-3.076044	2.864404	-1.083372
O	-1.783337	4.296681	-0.576867
O	1.287260	2.877941	3.192316
MG	-0.011520	4.268019	2.563605
O	3.452201	1.503666	1.856399
MG	2.161223	2.888819	1.292798
O	0.910443	4.298708	0.668607
MG	2.585989	1.439885	3.728768
O	3.821942	0.003932	4.287710
MG	4.543260	0.005790	2.486257
O	-1.322544	5.626509	1.972691
MG	-0.521711	5.551116	0.225820
O	-3.954738	-2.910458	0.799635
MG	-5.185718	-1.441822	0.209589
O	-1.768556	-4.303044	-0.580601
MG	-3.065896	-2.874100	-1.085553
O	-4.330564	-1.489342	-1.745300
MG	-2.611574	-4.270134	1.371589
O	-1.303627	-5.632983	1.967815
MG	-0.502990	-5.554143	0.221317
O	-6.431381	-0.011484	-0.365304
MG	-5.557727	-0.008468	-2.075064
MG	-0.436892	-0.000840	-0.004650
IR	1.762263	-1.326659	-1.863668
IR	1.755358	1.335985	-1.862761
C	3.204166	0.007528	-1.230749
O	4.305545	0.010322	-0.755020
C	1.995066	0.005761	-3.393128
C	0.146150	1.970472	-2.772300
C	2.934825	2.809556	-2.152073
C	2.951103	-2.793212	-2.150960

C	0.156575	-1.969664	-2.774227
O	2.116046	0.006351	-4.568693
O	-0.685231	-2.309943	-3.484029
O	3.693947	-3.638047	-2.406274
O	-0.697960	2.305770	-3.481870
O	3.670794	3.659698	-2.409829



## Supporting References

1. Newville, M., IFEFFIT: interactive XAFS analysis and FEFF fitting. *J. Synchrotron Radiat.* **2001**, *8*, 322-324.
2. Vaarkamp, M.; Linders, J. C.; Koningsberger, D. C., A New Method for Parameterization of Phase-Shift and Backscattering Amplitude. *Physica. B* **1995**, *208*, 159-160.
3. Parr, R. G.; Yang, W., Density-Functional Theory of Atoms and Molecules. Oxford University Press, New York: **1989**.
4. Chai, J. D.; Head-Gordon, M., Long-range Corrected Hybrid Density Functionals with Damped Atom-atom Dispersion Corrections. *Phys. Chem. Chem. Phys.* **2008**, *10*, 6615-6620.
5. Godbout, N.; Salahub, D. R.; Andzelm, J.; Wimmer, E., Optimization of Gaussian-Type Basis-Sets for Local Spin-Density Functional Calculations .1. Boron through Neon, Optimization Technique and Validation. *Can. J. Chem.* **1992**, *70*, 560-571.
6. Prascher, B. P.; Woon, D. E.; Peterson, K. A.; Dunning, T. H.; Wilson, A. K., Gaussian Basis Sets for Use in Correlated Molecular Calculations. VII. Valence, Core-valence, and Scalar Relativistic Basis Sets for Li, Be, Na, and Mg. *Theor. Chem. Acc.* **2011**, *128*, 69-82.
7. Figgen, D.; Peterson, K. A.; Dolg, M.; Stoll, H., Energy-consistent Pseudopotentials and Correlation Consistent Basis Sets for the 5d Elements Hf-Pt. *J. Chem. Phys.* **2009**, *130*, 164108.
8. Frisch, M. J.; Trucks, G. W.; Schlegel, H. B.; Scuseria, G. E.; Robb, M. A.; Cheeseman, J. R.; Scalmani, G.; Barone, V.; Petersson, G. A.; Nakatsuji, H.; Li, X.; Caricato, M.; Marenich, A. V.; Bloino, J.; Janesko, B. G.; Gomperts, R.; Mennucci, B.; Hratchian, H. P.; Ortiz, J. V.; Izmaylov, A. F.; Sonnenberg, J. L.; Williams; Ding, F.; Lipparini, F.; Egidi, F.; Goings, J.; Peng, B.; Petrone, A.; Henderson, T.; Ranasinghe, D.; Zakrzewski, V. G.; Gao, J.; Rega, N.; Zheng, G.; Liang, W.; Hada, M.; Ehara, M.; Toyota, K.; Fukuda, R.; Hasegawa, J.; Ishida, M.; Nakajima, T.; Honda, Y.; Kitao, O.; Nakai, H.; Vreven, T.; Throssell, K.; Montgomery Jr., J. A.; Peralta, J. E.; Ogliaro, F.; Bearpark, M. J.; Heyd, J. J.; Brothers, E. N.; Kudin, K. N.; Staroverov, V. N.; Keith, T. A.; Kobayashi, R.; Normand, J.; Raghavachari, K.; Rendell, A. P.; Burant, J. C.; Iyengar, S. S.; Tomasi, J.; Cossi, M.; Millam, J. M.; Klene, M.; Adamo, C.; Cammi, R.; Ochterski, J. W.; Martin, R. L.; Morokuma, K.; Farkas, O.; Foresman, J. B.; Fox, D. J. *Gaussian 16 Rev. B.01*, Wallingford, CT, **2016**.
9. Zhou, X. F.; Pulay, P.; Hargitai, R.; Stirling, A.; Mink, J., Complete Assignment of Vibrational-Spectra of 1,5-Cyclooctadiene - a Theoretical and Experimental Infrared and Raman-Study. *Spectrochim. Acta. A* **1993**, *49*, 257-270.
10. (a) Barna, G. G.; Butler, I. S., Vibrational-Spectra of 1,5-Cyclooctadiene, Di-Mu-Chlorobis[(1,5-Cyclooctadiene)Rhodium(I)], Di-Mu-Chlorobis[(1,5-Cyclooctadiene)Copper(I)] and Bis(1,5-Cyclooctadiene)Copper(I) Perchlorate. *J. Raman Spectrosc.* **1978**, *7*, 168-172; (b) Uson, R.; Oro, L. A.; Cabeza, J. A.; Bryndza, H. E.; Stepro, M. P., Dinuclear Methoxy, Cyclooctadiene, and Barrelene Complexes of Rhodium(I) and Iridium(I). *Inorg. Syn.* **1985**, *23*, 126-127; (c) Wertz, D. W.; Moseley, M. A., Vibrational Study of the Metal-Olefin Bond in 1,5-Cyclooctadiene Complexes of Rhodium(I), Palladium(II), and Platinum(II). *Inorg. Chem.* **1980**, *19*, 705-708.
11. (a) Boccuzzi, F.; Chiorino, A.; Manzoli, M., FTIR Study of Methanol Decomposition on Gold Catalyst for Fuel Cells. *J. Power Sources* **2003**, *118*, 304-310; (b) Dastoor, H. E.; Gardner, P.; King, D. A., Identification of 2 Tilted Adsorbed Mu-2-Methoxy Species on Ni(110) Using Rairs. *Chem. Phys. Lett.* **1993**, *209*, 493-498.
12. Aydin, C.; Lu, J.; Browning, N. D.; Gates, B. C., A "Smart" Catalyst: Sinter-Resistant Supported

Iridium Clusters Visualized with Electron Microscopy. *Angew. Chem. Int. Ed.* **2012**, *51*, 5929-5934.

13. Tabrizi, D.; Pannetie, G., Radiocrystallographic Study of Di-Mu-Methoxy-Bis(Pi-Cyclooctadiene-1,5)Diiridium [(COD-1,5)IrOCH<sub>3</sub>]<sub>2</sub>. *J. Less-Common Met.* **1971**, *23*, 443-&.

14. Hanlan, L.; Ozin, G., Synthesis using transition metal diatomic molecules. Dirhodium octacarbonyl and diiridium octacarbonyl. *J. Am. Chem. Soc.* **1974**, *96*, 6324-6329.

15. Chen, M.; Dyer, J. E.; Gates, B. C.; Katz, A.; Dixon, D. A., Structures and Stability of Ir<sub>n</sub>(CO)<sub>m</sub>. *Molecular Physics* **2012**, *110*, 1977-1992.